DELFT UNIVERSITY OF TECHNOLOGY

A novel concept for shallow water munitions removal – development and workability analysis

by

Vince in het Panhuis

A thesis submitted in fulfillment for the
degree of Master of Science

Offshore & Dredging Engineering
Delft University of Technology

November 24, 2016

A novel concept for shallow water munitions removal – development and workability analysis

Author:
Vince in het Panhuis

Thesis Committee:

TU Delft:
Prof. Dr. ir. C. van Rhee
Dr. ir. S. Miedema
Ir. K. Visser

Boskalis:
Ir. S. Henrion
Ir. M. Biesheuvel

This is an adjusted version of the full thesis report.

Abstract

As a result of past world wars and the dumping of munition at designated dumping areas, residual military ordnance are found on and in the seabed, especially in the Wadden Sea, North Sea and Baltic Sea. Of the estimated 1.5 million tons of military ordnance, roughly ten percent is classified as Unexploded Ordnance (UXO). There are three main arguments for removing the military ordnance: environmental protection, human safety and project related. Current study will focus on the project related removal of munition, specifically for offshore wind cable installation projects. Recovery of UXO is often preferred over redirection of the cable route due to cost savings. Current state of the art methods use dedicated clearance ROV's and divers to remove the munition ordnance. However, these methods prove to be dangerous, inefficient or even impossible to use in shallow water areas (0-10 m) with strong tidal currents. The objective of current study is to develop a remotely-operated munitions detection and removal concept for use in coastal water areas and assess its feasibility.

First, a programme of requirements for the novel concept is obtained. During a systematic ideation process, fifteen different conceptual ideas are conceived and compared in a multi-criteria analysis from which the most promising concept is chosen: an excavator carrying a munitions toolskid on a moored pontoon.

The second part of the study focuses on assessing the feasibility of the proposed concept for two project sites. Specifically for this study, the workability in waves is assessed. Limiting criteria are defined for two critical components on the munitions toolskid to ensure a safe operation; the motion amplitude of the detection coils, limited to X vertical motion and the motion amplitude of the manipulators, limited to X absolute motion. The latter limit is based on user experience of existing ROV operations and is thus subject to interpretation. The motion amplitude of manipulator and detection coils is modelled by combining three sources of motion; backlash mobilization in the excavator, bending deflection of the excavator arm and wave induced pontoon motions. Three different types of mooring are modelled; gravity spuds, backhoe-type spuds (i.e. preloaded spuds) and a jack-up system.

Results of the workability assessment for two case studies show that the gravity spuds pontoon is not a feasible solution, mainly due to the freedom of heaving and pitching. Both defined motion limits are exceeded by more than X. When using backhoe spuds or jack-up system, the criterion for the scanning coils is satisfied. The criterion for the manipulators is slightly exceeded by respectively X and X absolute motion for the backhoe and jack-up system. It can be concluded that none of the assessed solutions is workable if an exceedance of the motion limit for the manipulator is strictly prohibited. However, considering the exceedance of the limit is slight and the motion limit of the manipulator should be interpreted as an indication, the backhoe and jack-up system may prove to be workable solutions. Reassessment of the limiting criterion for the manipulator is required to give insight if a slight exceedance of the limit is allowable.

Acknowledgements

This thesis of course could not have come about without the support of few people, whom I like to thank for that. I would first like to thank my daily supervisors Sebastian Henrion and Mark Biesheuvel of Boskalis for their guidance, support and encouragement during my graduation work. Whenever needed, they showed me the bigger picture of the project and helped me keep the relation with the practical aspects of the project. I would like to thank my TU Delft supervisor, Sape Miedema, for his support during my thesis. He consistently allowed this study to be my own work, but steered me in the right the direction whenever he thought I needed it. I would also like to thank my professor, Cees van Rhee, for the valuable and constructive progress meetings.

I would also like to thank the Boskalis MDD team who were involved in helping me understand the fundamentals of ship hydrodynamics and simulations. Special thanks to Oscar Sainz Avila, whose "door" was always open for a discussion on the matter. Without their participation and input, the workability assessment of this study could not have been successfully conducted. A big thanks to my fellow graduation students, for the relaxed atmosphere in the office during my time at Boskalis.

Finally, I express my gratitude to my parents and to my girlfriend for providing me with unfailing support and encouragement throughout my years of study. This accomplishment would not have been possible without them.

Thank you all,

Vince

Contents

List of Figures

List of Tables

Nomenclature

Abbreviations

AUV	Autonomous Underwater Vehicle
BSH	Bundesamt fur Seeschiffahrt und Hydrographie
COG	Center Of Gravity
DP	Dynamic Positioning
EM	Electro-Magnetic
EOD	Explosive Ordnance Disposal
MCA	Multi-Criteria Analysis
RAO	Response amplitude operator
ROV	Remote Operated Vehicle
SWAN	Simulating Waves Nearshore
UXO	Un-eXploded Ordnance

Roman Symbols

A	Projected area normal to force direction	m^2
A_r	Reference cross sectional area	m^2
A_w	Nominal cross sectional area	m^2
A_{kj}	Added mass coefficient matrix	-
B_{kj}	Damping coefficient matrix	-
C_a	Added mass coefficient	-
C_d	Drag coefficient	-
C_m	Inertia coefficient	-
C_{kj}	Hydrodynamic and static intertia restoring matrix	-
D_i	Inner diameter	m
D_o	Outer diameter	m
E	Young's modulus	Nm^{-2}
F_i	Point load	N
F_{ex}	Wave exciting forces	N
F_k	Hydrodynamic forces	N
F_m	Mooring forces	N
F_r	Radiation forces	N
F_s	Hydrostatic forces	N

F_v	Viscous forces	N
F_{w1}	First order wave forces	N
F_{w2}	Second order wave forces	N
GM	Metacentric height	m
H	Wave height	m
H_m	Maximum wave height in a sea state	m
H_s	Significant wave height	m
I	Second moment of area	m
L	Length	m
L_b	Length of the beam	m
L_s	Length of the free end of the spuds	m
L_w	Length of wire	m
L_{sk}	Length from the top to the bottom spudkeeper	m
M	Applied moment	Nm^{-1}
M_{kj}	Body inertia matrix	-
N	Number of waves in the operational window	-
N_w	Number of wires	m
P_h	Hydraulic power	kW
Q	Hydraulic flow	lpm
R	Reaction force	N
S	Projected area normal to force direction	m^2
S_ζ	Spectral density	Nm^{-2}
S_{js}	JONSWAP spectral density	$\mathrm{m}^2\mathrm{Hz}^{-1}$
T	Draft	m
T_l	Laden draft	m
T_m	Mean wave period	s
T_p	Peak wave period	s
T_w	Wave period	s
T_z	Zero up-crossing wave period	s
V_r	Reference volume	m^3
a_b	Arm length of the boom	m
a_s	Arm length of the stick	m
d	Water depth	m
d_{min}	Minimum operating water depth	m

h	Duration of operation	h
k	Wave number	-
k_h	Horizontal stiffness	Nm^{-1}
k_z	Vertical stiffness	Nm^{-1}
k_{xx}	Radius of gyration around x-axis	tm^2
k_{yy}	Radius of gyration around y-axis	tm^2
k_{zz}	Radius of gyration around z-axis	tm^2
m	Spectral moment	-
p	Pressure	Nm^{-2}
u_x	Horizontal wave particle velocity	ms^{-1}
u_z	Vertical wave particle velocity	ms^{-1}
v	Horizontal wave particle velocity	ms^{-1}
v_c	Current velocity	ms^{-1}
v_w	Wind velocity	ms^{-1}
w	Excavator tip motion amplitude	m

Greek Symbols

α	Angle between the boom and stick	deg
δ_b	Boom deflection	m
δ_s	Stick deflection	m
δ_{tot}	Total deflection	m
ϵ_t	Target position error	m
ϵ_{ts}	Toolskid position error	m
η_c	Efficiency of hydraulic circuit	-
λ	Wave length	m
∇_l	Laden displacement	t
ω	Wave angular frequency	rads^{-1}
ρ_w	Density of seawater	kgm^{-3}
σ	Spectral data constant	-
θ_b	Rotation of the boom due to backlash	deg
θ_s	Rotation of the stick due to backlash	deg
ε	Phase angle	-
ζ	Surface elevation	m
ζ_a	Wave amplitude	m

Chapter 1

Introduction

1.1 Context

As a result of past world wars and the dumping of ammunition at designated dumping areas, residual military ordnance are found on and in the seabed, especially in the Wadden Sea, North Sea and Baltic Sea. Experts estimate that ten percent of the 1.5 million tons of military ordnance deployed during the World Wars has failed to explode in German territorial waters alone [1]. The unexploded ordnance (UXO) include aerial bombs weighing hundreds of kilograms, shells, torpedoes, high-explosive bombs, bombs of chemical origin, hand grenades and small ammunition, for a total of more than 50 million individual items (see figure 1.1).

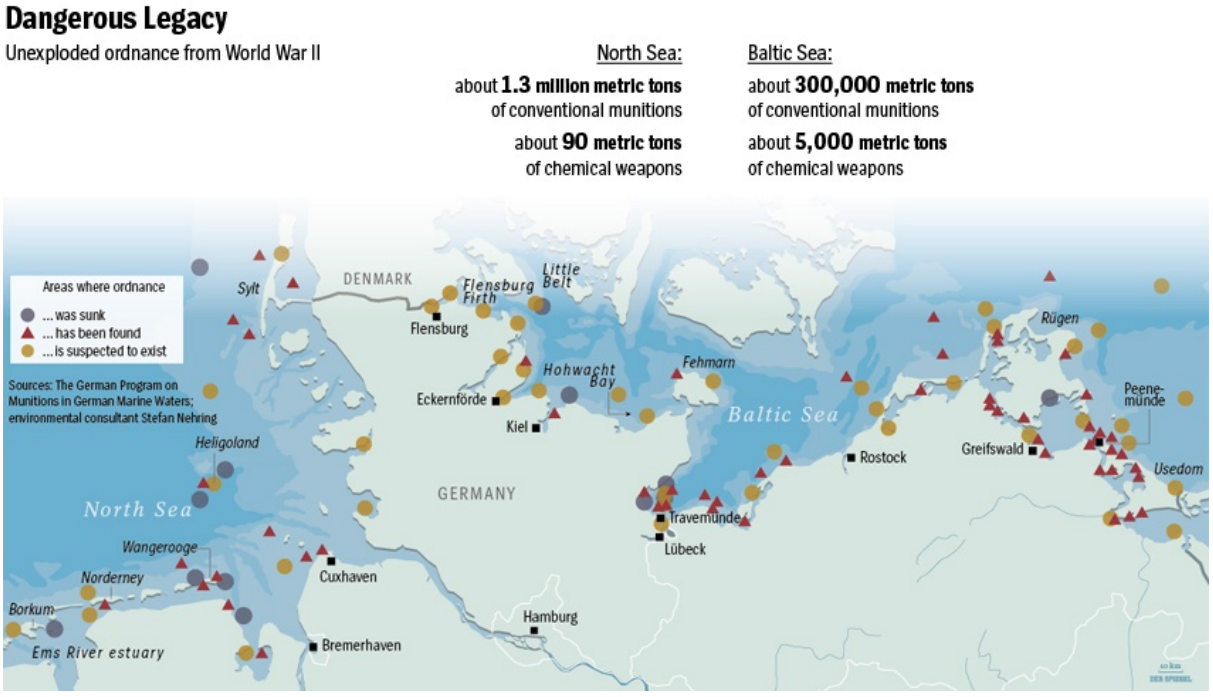

FIGURE 1.1: Overview map of underwater munition locations in German waters. Courtesy of the German program on munitions in German waters.

The three main agruments for removal of the underwater munitions are:

- Project related (Wind-farms, subsea cables, pipe laying projects, oil, gas and mineral exploration and capital dredging project)
- Environmental / Ecological
- Human safety

Current study will focus on the project related aspects of the removal of underwater munitions. Specifically, the munitions will be removed to clear the route for offshore cable-laying operations and development of offshore wind farms. The global offshore wind market has grown in average more than 30 % annually in the last five years and is expected to keep growing in the coming years [2]. Removal of the UXO is often preferred over redirection of the cable route due to cost savings. An example of recent UXO remediation work is the Riffgate offshore wind farm. During construction work, 2.7 metric ton of munitions where discovered and salvaged [3].

Some of the underwater munitions is of chemical origin. Because of rust degradation these underwater munitions can release toxic chemicals which pollute and destroy the marine environment, hence the environmental reason for removing the munition. The chemicals, for example phosphor and mustard gas, are destructive for the marine ecosystem and the animals that live in it. Removal of munitions will therefore ensure a cleaner and healthier marine environment.

Lastly, the human safety argument for removing munitions is to reduce the chance of munition-related human accidents. According to [4], there are three types of danger that munitions dumped at sea can cause to human life:

1. Direct physical contact with either chemical or conventional munitions.
2. Contamination of marine organisms and the environment in proximity of dumped munitions which could in the long run lead to harmful concentration of toxic waste in human food chains.
3. Spontaneous explosions which can be life threatening.

Direct physical contact or disturbance of munitions can occur with various marine activities for example fishing and diving. Still often fishermen are injured after detonation of an UXO pulled on board in their nets. Recently in 2005, three fishermen lost their lives in the southern part of the North Sea when a World War II bomb exploded on board their fishing vessel after having been hauled aboard in their nets [5].

1.2 State of the Art

1.2.1 Munitions recovery in general

In cases of buried unexploded ordnance a desk study is done by interpretation of available historical data. Modern techniques can combine geophysical and survey methods with modern electromagnetic and magnetic detectors. This provides mapping of munition contamination with the aim to better target subsequent excavations, reducing the cost of digging on every metallic contact and speeding the clearance process. [6]

Currently, there is a lot of research into the detection and discrimination of munitions from scrap metal [7][8]. Much of the cost of munitions removal comes from removing non-explosive items that the metal detectors have identified, so improved discrimination is critical. New techniques such as munition reconstruction from magnetic data and better noise reduction techniques will reduce costs. (Electro)magnetometer probes can detect UXO and provide geotechnical data before removal is carried out. Probing is mostly done by hand-held, sled-mounted or cart mounted tools (figure 1.2a). For deep buried UXO, an intrusive survey might be required (figure 1.2b).

If an UXO is found, it needs to be dismantled. Many techniques exist for making safe of a bomb or munition. Selection of a technique depends on several variables. The greatest variable is the proximity of the munition to people or critical facilities. EOD personnel have many tools for remote operations, one of which is remotely controlled vehicle, also known as the "Wheelbarrow". The wheelbarrow can help to get an idea of what the munition or device is [9] (figure 1.3a and 1.3b).

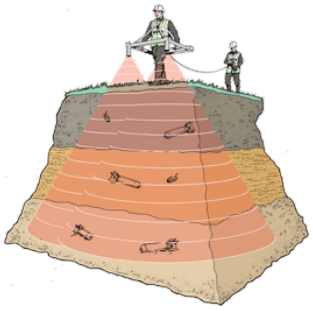

(A) Hand-held tools for scanning.

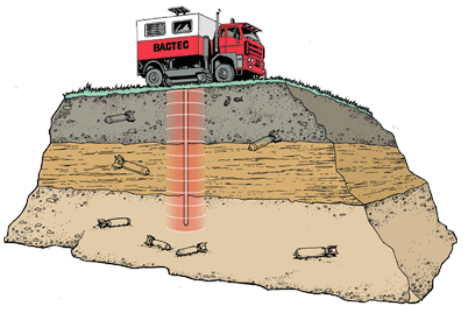

(B) Intrusive survey method.

FIGURE 1.2: Examples of UXO detection methods on land

(A) Remotely controlled vehicle or 'Wheelbarrow'.

(B) Wheelbarrow putting UXO in a containment vessel.

FIGURE 1.3: Disposal techniques

1.2.2 Offshore munitions recovery

Also for offshore UXO survey, a desk study of historical data is carried out. A towfish, remote operated towed vehicle (ROTV) or autonomous underwater vehicle (AUV) equipped with magnetometers, electromagnetic and sonar scanners is used to survey the seabed and obtain an approximate location of possible UXO (figure 1.4a).

Current methods which are used for underwater UXO recovery are EOD diving and removal by ROV. Diving requires a team of EOD certified divers to manually locate and remove each individual target. After the target has been marked by a survey, the divers enter the water with an underwater magnetic sensor to precisely pinpoint the target. Once the target is located, the diver begins the investigation and recovery process. Either using his hands or hand tools, he uncovers the item. Targets buried more than 1 m typically cannot be successfully recovered using this approach regardless of whether the bottom sediments are sand, shell, silt/mud, or clay. Divers have access only to small hand tools. After the target is uncovered, the diver identifies the target visually if possible, or by feel if visibility is limited. The UXO supervisor then determines if the item can be safely moved or whether it must be disposed of on location. The removal is done by crane-lifting or with the help of an array of electromagnets, as shown in figure 1.4b.

There are few specialized underwater removal methods that don't involve diver intervention. One example is the Boskalis Schilling HD ROV outfitted with manipulators, a dredge pump and metal detection coils. This method is currently used for munitions recovery in benign sea states. Another example is the ROUMRS (Remotely operated underwater munitions recovery system) by Ordnance Reef Technology [10]. This is similar to Boskalis' ROV solution and consist of an off-the-shelf ROV that is equipped with force-feedback manipulators and a storage skid for recovered UXO. It recovered 74 pieces of UXO's and 2,300 small arms munitions, clearing most of the area off the Waianae Coast of Hawaii.

Another recently developed concept is a small muntion recovery work boat developed by the Environmental Security Technology Certification Program [11]. The work boat is anchored next

(A) Deployment of towfish with electromagnetic scanning equipment.

(B) UXO removal with magnets.

FIGURE 1.4: Examples of offshore UXO removal equipment

to a barge. It is stabilized by two spuds that are driven into the seabed. A deck crane is used to lower a cylindrical shroud onto the target position and a remotely operated dredge is used to excavate the sediment from the hole to expose the target. The target is remotely examined using either a camera or an imaging sonar system to identify the target. If a supervisory munitions technician determines that the target is safe to recover, it is remotely retrieved using an array of electromagnets. The tool is designed for lakes lagoons with negligible wave action.

1.3 Problem Identification and Objectives

Current technologies are well developed if the water depth is greater than 10 meters and the sea state is benign. However, when recovery in water depths between 1 and 10 meters is required, in challenging coastal environments, the methods prove to be dangerous and inefficient or even impossible to use. The following list gives the reasons why a new approach is preferred over current methods for shallow water UXO recovery in water depths of 1 - 10 meter.

- Recovery of munitions with the help of EOD qualified divers is dangerous work and proves to be laborious for deep buried targets. Furthermore the workability of divers in waves and current is very limited. Thus, a diverless removal method is preferred.
- Some of the shallow water areas are located in tidal bassins and channels. The current velocities in these areas are significant. This makes remediation of munition by current ROV's impossible since screw-propelled vehicles can not keep station in high current velocities.
- A lot of munition targets are located in areas where it is too shallow for current vessel- and ROV-based munition removal tools to work in. These methods simply require a minimum amount of water depth.

Objectives
The proposed objective for this study are:

1. Develop a remotely-operated munitions detection and removal concept, to create an safe, reliable and cost-efficient method for use in recovering suspicious targets in challenging coastal water areas.

2. Assess the feasibility of the proposed concept.

1.4 Thesis Approach

To reach the objectives of this study, a systematic approach is used. It is important to have a detailed design procedure in order to find satisfactory solutions and to ensure timely and efficient concept development. This procedure must be flexible and at the same time be capable of being planned, optimised and verified.

The approach used for this study is displayed in figure 1.5. The study is divided in two parts; a concept study and a proof of concept. These parts are again divided in several steps. The study is initiated with a introduction where the problem and requirements for the new concept are stated. The requirements are based on stakeholders wishes and demands, environmental data (chapter 3) and a functional breakdown of the tool. A programme of requirements is obtained at the end of chapter 4. Once the details of the design are clearly identified, the concept ideation process is initiated. Multiple concept alternatives are generated in chapter 5 to achieve the design goals and satisfy the requirements. With the help of a multi-criteria analysis (MCA), the most promising alternative(s) are selected for further analysis in chapter 6. The chosen solution at the end of chapter 6 may prove unworkable for any number of reasons and may require redefining the problem, collecting more information, or generating different solutions. This continuous iterative process is represented in the figure as an iteration block. The overall layout and embodiment of the chosen concept will be elaborated in chapter 7.

The second part of this study is the proof of concept. Specifically for this study, the workability of the concept in waves is tackled. Chapter 8 defines the approach that is used too determine the workability. Chapter 9, 10 and 11 are the main part of the proof of concept. In these chapters, the workability of the proposed concept is evaluated with the help of several theoretical models. Finally, conclusive remarks and recommendations are summarized in chapter 12.

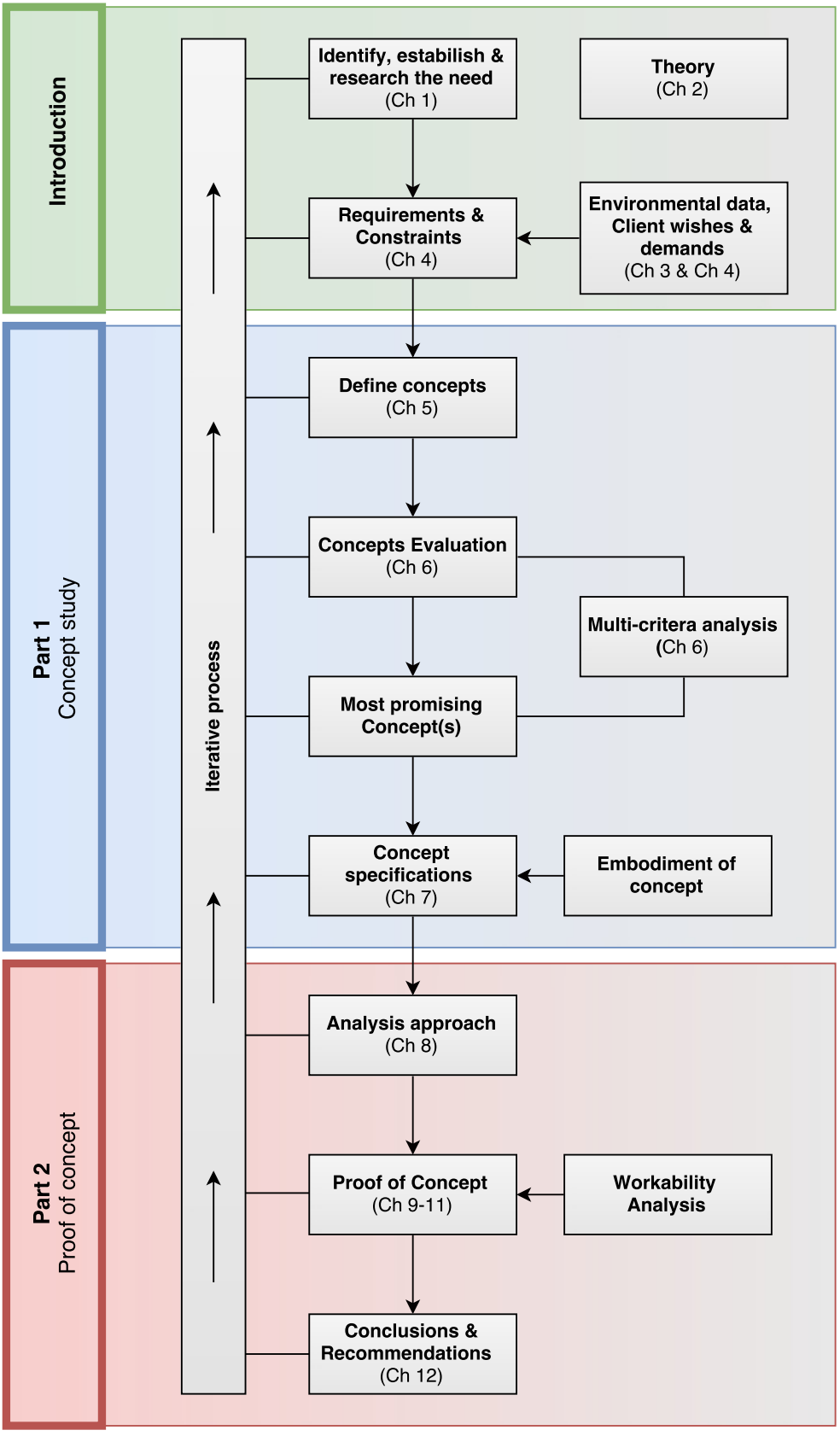

FIGURE 1.5: Chart of the approach of current study.

Chapter 2

Theory

In this chapter the fundamentals of the theory on waves (section 2.1), ship hydrodynamics (section 2.2) and the Morison equation (section 2.3) is given which will be used throughout the study. For a more elaborate explanation of the considered theory, reference is made to (Journée and Massie, 2000).

2.1 Waves

2.1.1 Regular waves

A regular wave in this study is described by the following wave characteristics:

Surface elevation:	$\zeta(x,t) = \zeta_a \sin(\omega t - kx)$
Wave amplitude:	$\zeta_a = 0.5 \cdot H$ in [m]
Wave height:	H in [m]
Wave period:	T in [s]
Wave length:	λ [m]
Wave angular frequency:	$\omega = 2\pi/T$ in [rad/s]
Wave number:	$k = 2\pi/\lambda$
Water depth:	d in [m]

A schematic view of a regular wave with its characteristic is depicted in figure 2.1.

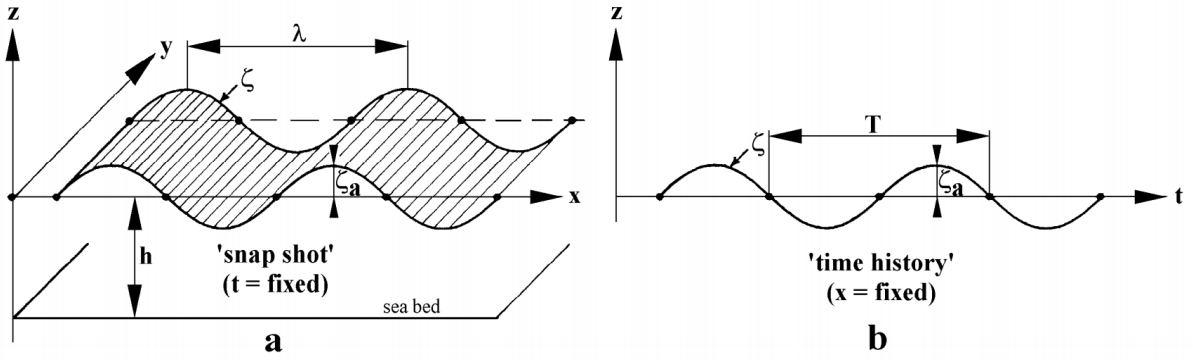

FIGURE 2.1: Description of a regular wave.

The wave particle velocities can be obtained from the velocity potential ϕ using linear wave theory. Linear wave (Airy wave) is considered as the simplest ocean wave, and is based on the assumption of homogeneous, incompressible, inviscid fluid and irrational flow. In addition, the

wave amplitude is assumed to be small compared to the wave length and water depth; hence the linear free surface condition is used [12]. The wave particle velocities in horizontal and vertical direction following linear wave theory are given by:

$$u_x = \hat{u}_x \sin(\omega t - kx) \qquad \text{and} \qquad u_z = \hat{u}_z \cos(\omega t - kx) \tag{2.1}$$

with the amplitudes:

$$\hat{u}_x = \omega\zeta_a \frac{\cosh[k(d+z)]}{\sinh(kd)} \qquad \text{and} \qquad \hat{u}_z = \omega\zeta_a \frac{\sinh[k(d+z)]}{\sinh(kd)} \tag{2.2}$$

With z the vertical coordinate, which is zero at the still water interface and $-d$ at the seabed. These velocities are the orbital wave particle velocities because they correspond to the motion of the particles in a closed circular of elliptical path. In deep water, i.e. when the $kd \to \infty$, the expressions for the velocity amplitudes $\hat{u}_x$ and $\hat{u}_z$ reduce to:

$$\hat{u}_x = \hat{u}_z = \omega\zeta_a e^{kz} \tag{2.3}$$

In deep water, the wave particles move in circles, with the radius of the circle at water surface equal to the wave amplitude a. These expressions show that the velocities decrease exponentially with increasing distance from the still water level as shown in figure 2.2. Water is assumed deep when $d \geq \frac{1}{2}\lambda$.

In very shallow water, i.e. when $kd \to 0$, the expressions of the amplitude reduce to:

$$\hat{u}_x = \frac{\omega\zeta_a}{kd} \qquad \text{and} \qquad \hat{u}_z = \omega\zeta_a(1 + \frac{z}{d}) \tag{2.4}$$

In very shallow water, the amplitude of the horizontal velocity component is constant over depth, whereas the vertical velocity amplitude varies linearly over depth as shown in figure 2.2. Equation (2.2),(2.3) and (2.4) give three different expressions for each velocity amplitude. The shallow water equation (2.4) can be used when $d \leq \frac{1}{20}\lambda$, the intermediate equation (2.2) when $\frac{1}{20}\lambda \leq d \leq \frac{1}{2}\lambda$ and the deep water equation (2.3) when $d \geq \frac{1}{2}\lambda$.

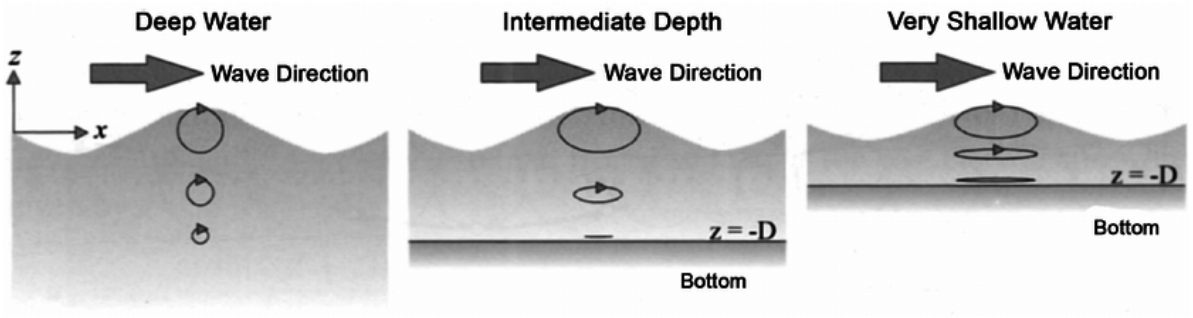

FIGURE 2.2: Orbital wave motions

Wave accelerations

The water particle accelerations follow directly from a differentiation of the velocity components (Eq (2.1)):

$$\dot{u}_x = \zeta_a \omega^2 \frac{\cosh(k(h+z))}{\sinh(kh)} \cdot \sin(kx - \omega t) \tag{2.5}$$

$$\dot{u}_z = -\zeta_a \omega^2 \frac{\cosh(k(h+z))}{\sinh(kh)} \cdot \cos(kx - \omega t) \tag{2.6}$$

Maximum Wave Height
It is often desirable to make a statistically-based guess as to the highest wave that can be expected in a certain time span. For this study, the maximum wave height during a munitions removal operation will be defined. With the help of the Rayleigh distribution, the maximum wave height in certain time span can be calculated by:

$$H_m = H_s \sqrt{\frac{\ln N}{2}} \tag{2.7}$$

in which N is the number of waves in the operational window expressed as:

$$N = 3600 \frac{h}{T_z} \tag{2.8}$$

Where h is the duration of an operation in hours and T_z the zero up-crossing wave period.

2.1.2 Irregular waves

A realistic image of the sea surface can be represented by using a linear superposition of regular wave components. For current study, it is assumed that all the wave components are in the same direction, i.e. unidirectional waves. A description of an irregular sea state can be obtained by measuring the wave surface elevation as a function of time. The following characteristics are obtained from a statistical analysis of the measurements:

- **Significant wave height** H_s
  The significant wave height is the mean of the highest third of the waves in a time-series of waves representing a certain sea state. This corresponds well with the average height of the highest waves in a wave group. H_s computed on the basis of a spectrum, is referred to as H_{m0}.
- **Mean wave period** T_m
  The mean wave period is the mean of all wave periods in a time-series representing a certain sea state.
- **Peak wave period** T_p
  The peak wave period is the wave period with the highest energy. The analysis of the distribution of the wave energy as a function of wave frequency for a time-series of individual waves is referred to as a spectral analysis.

- **Mean wave direction**
  The mean wave direction which is defined as the mean of all the individual wave directions in a time-series representing a certain sea state.

Since an irregular wave can be seen as the superposition of a series of sinusoidal waves, one can study the frequency characteristics of such an irregular signal using Fourier series analysis. Hereby, obtaining the amplitudes of each wave component in the signal. The wave amplitude ζ_a can then be expressed in a wave energy spectrum, depicted in figure 2.3. The expression for the wave energy spectrum is:

$$S_\zeta(\omega) \cdot d\omega = \frac{1}{2}\zeta_{a,n}^2 \tag{2.9}$$

Several theories exist that attempt to describe a wave spectrum in a standard form. For current study, the JONSWAP wave spectrum is used.

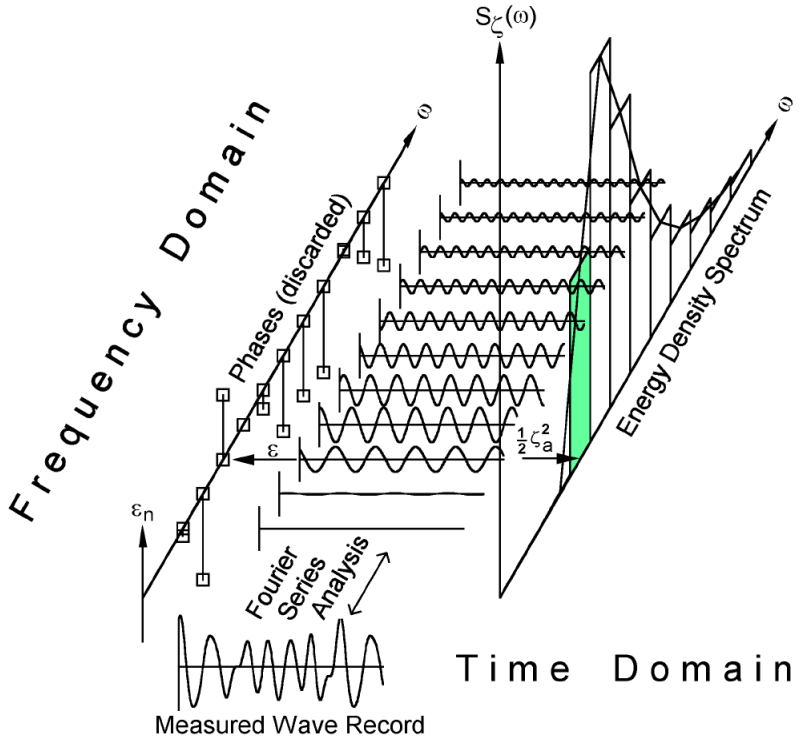

FIGURE 2.3: Schematic of how to obtain the energy density spectrum.

JONSWAP

Analysis of the extensive wave measurements data in the North Sea in 1968 and 1969 yielded a spectral formulation for fetch-limited (or coastal) wind generated seas. The spectrum is described by:

$$S_{js}(\omega) = \frac{320H_s^2}{T_p^4} \cdot \omega^{-5} \cdot \exp\left(-\frac{1950\omega^{-4}}{T_p^4}\right) \cdot \gamma^{\exp\left(-\frac{\omega}{\frac{f_p-1}{\sigma\sqrt{2}}}\right)^2} \tag{2.10}$$

where

H_s = Significant wave height [m]
T_p = Wave peak period [s]
f_p = Peak wave frequency = T_p^{-1} in [s]
ω = Angular wave frequency [rad/s]
σ = 0.07 for $\omega \leq \omega_p$
0.09 for $\omega > \omega_p$

In figure 2.4 the JONSWAP wave spectrum is depicted and compared with another spectrum, Bretschneider wave spectrum which is frequently used for open seas. The figure shows the more pronounced peaks of the JONSWAP spectra.

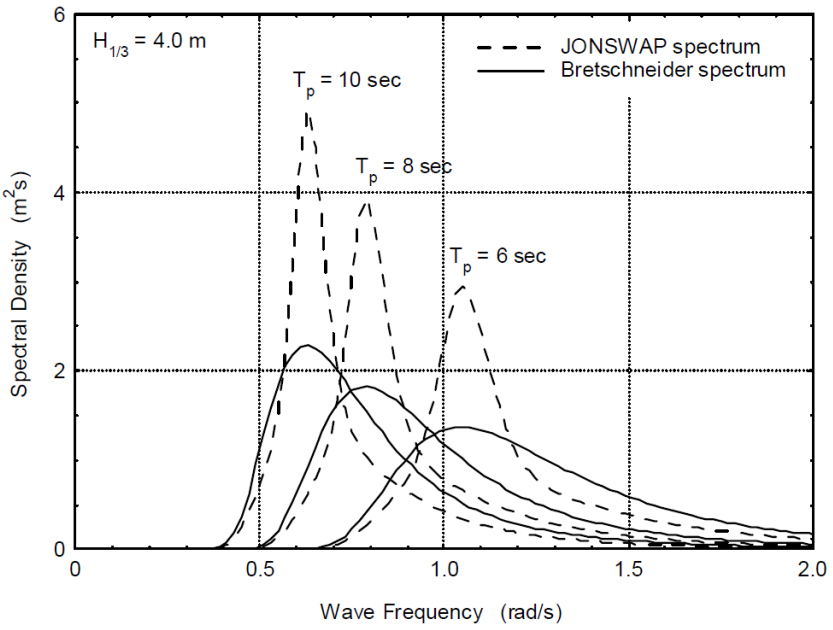

FIGURE 2.4: Graph showing the JONSWAP spectra compared to Breitschneider.

2.1.3 Shoaling and Breaking waves

As ocean waves approach the shore, they are affected by the decreasing depth, which causes gradual changes in wave speed, height and shape. These changes are usually referred to as wave shoaling. Very close to shore, shoaling causes wave height to increase and wavelength to decrease; hence, at some point, waves become too steep and break. The surfzone extends from the point where waves start to break to shore, and this is a region of high vorticity, turbulence, and dissipation for the wave flow. The proposed concept will be working in or near the surf zone. To model breaking waves, a sophisticated fully non-linear wave model would be required. This is out of scope of current thesis, since it would require an elaborate CFD model to calculate the wave loads and thus the ship motions. However, assuming linear wave theory usually gives a good approximation of the wave loads, even when working in the surf zone [13].

2.2 Ship dynamics

2.2.1 Definitions

The harmonic 6 rigid body motions are defined by 3 translations and 3 rotations of the body's center of gravity (COG) as follows (see figure 2.5):

$$x = x_a \cos(\omega t + \varepsilon_{x,\zeta}) \quad \text{(Surge)} \tag{2.11}$$

$$y = y_a \cos(\omega t + \varepsilon_{y,\zeta}) \quad \text{(Sway)} \tag{2.12}$$

$$z = z_a \cos(\omega t + \varepsilon_{z,\zeta}) \quad \text{(Heave)} \tag{2.13}$$

$$\phi = \phi_a \cos(\omega t + \varepsilon_{\phi,\zeta}) \quad \text{(Roll)} \tag{2.14}$$

$$\theta = \theta_a \cos(\omega t + \varepsilon_{\theta,\zeta}) \quad \text{(Pitch)} \tag{2.15}$$

$$\psi = \psi_a \cos(\omega t + \varepsilon_{\psi,\zeta}) \quad \text{(Yaw)} \tag{2.16}$$

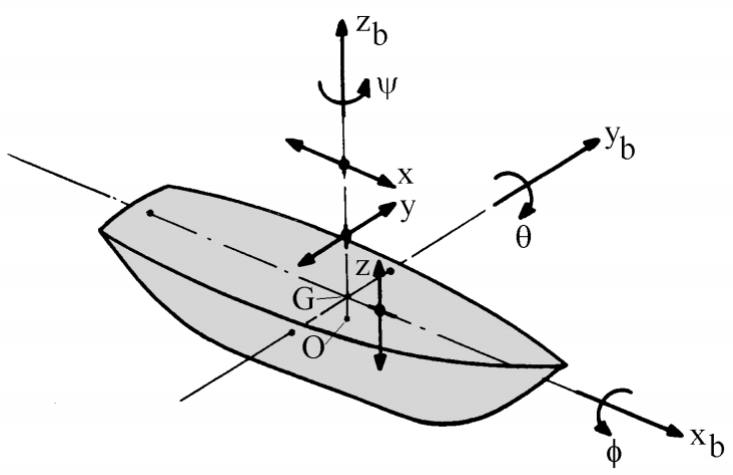

FIGURE 2.5: Definition of ship motions.

Knowing the motions around the body's COG one can calculate the motions in any point on the structure by employing the superposition principle. For small angles, the transformation matrix from the body-bound coordinate system to the steadily translating coordinate system is given by:

$$\begin{bmatrix} x \\ y \\ z \end{bmatrix} = \begin{bmatrix} 1 & -\psi & \theta \\ \psi & 1 & -\phi \\ -\theta & \phi & 1 \end{bmatrix} \cdot \begin{bmatrix} x_b \\ y_b \\ z_b \end{bmatrix} \tag{2.17}$$

Using the equation the absolute harmonic motion of a certain point $P(x_b, y_b, z_b)$ relative to the COG of the vessel can be determined.

2.2.2 Equation of motion

The response of a ship to waves is described by:

$$\sum_{j=1}^{6} M_{kj}\ddot{x}_j = F_k^e \tag{2.18}$$

Where M_{kj} is the body inertia matrix including moments of inertia for rotational modes of the vessel. $\ddot{x}$ represents the rigid body acceleration for all six degrees of freedom (surge, sway heave, roll, pitch and yaw). The right hand side gives the hydrodynamic forces and moments acting on the body, divided in the following components:

$$F_k^e = F_r + F_w + F_v + F_s + F_m \tag{2.19}$$

in which:

- F_r = **Radiation forces** appearing due to change in momentum of the fluid because of the body motion, further decomposed to added-mass forces (proportional to body's accelerations) and damping forces (proportional to body's velocities).
- F_{w1} = **First order wave forces** separated into the Froude-Krylov forces and the diffraction forces. The Froude–Krylov force is the force introduced by the unsteady pressure field generated by undisturbed waves. The diffraction force is due to the floating body disturbing the waves.
- F_{w2} = **Second order wave drift forces**, slowly varying wave loads.
- F_v =**Viscous forces** which are non-linear damping forces due to non-conservative phenomena of energy dissipation (skin friction, flow separation phenomena).
- F_s = **Hydrostatic forces** or restoring 'spring' forces, proportional to body's translations and rotations. The non-zero spring coefficients are in heave roll and pitch.
- F_m = **Mooring forces**, in case the floating body is moored.

For more detailed information about the above forces reference is made to [12]. The forces and moments follow from an integration of the pressure, p, over the submerged surface, S, of the floating body. Equation (2.18) can also be written as:

$$\sum_{j=1}^{6}(M_{kj} + A_{kj})\ddot{x}_j + B_{kj}\dot{x}_j + C_{k,j}x_j = F_{ex,k} \qquad \text{Where k = 1,2, ... 6} \tag{2.20}$$

in which:

M_{kj} = Body inertia matrix including moments of inertia for rotational modes
A_{kj} = Added mass coefficient matrix
B_{kj} = Damping coefficient matrix
C_{kj} = Hydrodynamic and static inertia restoring matrix including mooring stiffness
$F_{ex,k}$ = Wave exciting forces and moments

The expression for the frequency dependent equation of (2.20) where $x_j = \hat{x}_j \cdot e^{-i\omega t}$ and $F_{ex} = \hat{F}_{ex} \cdot e^{-i\omega t}$ is:

$$\left[\sum_{j=1}^{6} -\omega^2(M_{kj} + A_{kj}) - i\omega B_{kj} + C_{k,j}\right]\hat{x}_j = \hat{F}_{ex,k} \tag{2.21}$$

in which:

$\hat{x}_j$ = Amplitude of the periodic motions of the vessel
$\hat{F}_{ex,k}$ = Amplitudes of wave exciting forces and moments

2.2.3 Ansys AQWA

Ansys AQWA, which is based on 3D panel method, is selected to compute wave forces in the frequency domain for current study. The method is a numerical method to calculate the potential flow around a body, based on the Green's integral theorem. In this theorem, the three-dimensional linear homogeneous differential equation is transformed into a two-dimensional integration equation. Thus, the three-dimensional potential equation can be transformed to a surface integral equation, known as Green's identity [14]. To solve the integral equation numerically, the ship body is divided in panels, shown for the pontoon used in this study in 2.6. The boundary conditions to be applied to the problem are linearised and they determine either the potential or the normal velocity on each panel. Hydrodynamic forces are determined from pressure integration and the motion responses of the vessel are determined (i.e. Response Amplitude Operators, RAO's). RAO's are effectively transfer functions used to determine the effect that a sea state will have on the motions of a ship. For example, equation (2.22) shows the frequency dependent heave RAO:

$$RAO_z(\omega) = \frac{z_a}{\zeta_a}(\omega) \tag{2.22}$$

Where z_a is the heave amplitude and ζ_a is the wave amplitude for a certain wave frequency.

The 3D panel method has a couple of limitations. The method is restricted to arbitrarily shaped bodies with zero forward speed, which is the case in current study. Furthermore, the method assumes that the oscillation amplitudes of the fluid and body are small relative to the cross-section dimensions of the body.

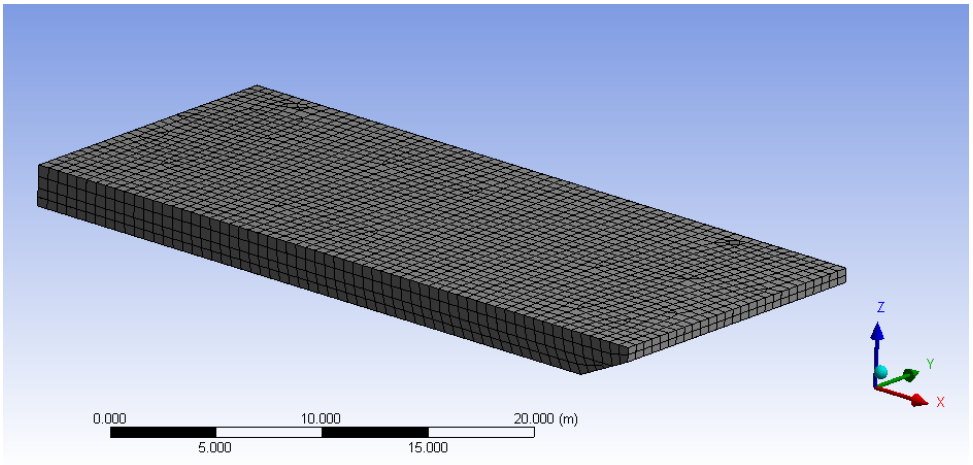

FIGURE 2.6: Screendump of a pontoon panel mesh in AQWA.

2.2.4 Response in irregular waves

Once the transfer functions (RAO's) between wave energy and motion (component) energy are known, one can transform any wave energy spectrum to a corresponding motion energy spectrum. The wave energy spectrum was defined in section (2.9). For example the heave response is defined as:

$$S_z(\omega) = \left|\frac{z_a}{\zeta_a}(\omega)\right|^2 \cdot S_\zeta(\omega) \tag{2.23}$$

The principle of this transformation of wave energy to response energy is shown in figure 2.7 for the heave motions considered in the equation. The moments of the heave response spectrum are given by:

$$m_{n,z} = \sum_0^\infty S_z(\omega) \cdot \omega^n \cdot d\omega \tag{2.24}$$

where n = 0,1,2 provides the respectively the area, first moment and the moment of inertia of the spectral curve. The significant motion amplitude can be calculated from the spectral density function of the motions. For example, the significant heave amplitude, defined as the mean value of the highest one-third part of the amplitudes, is:

$$z_{sign} = 2\sqrt{m_{0,z}} \tag{2.25}$$

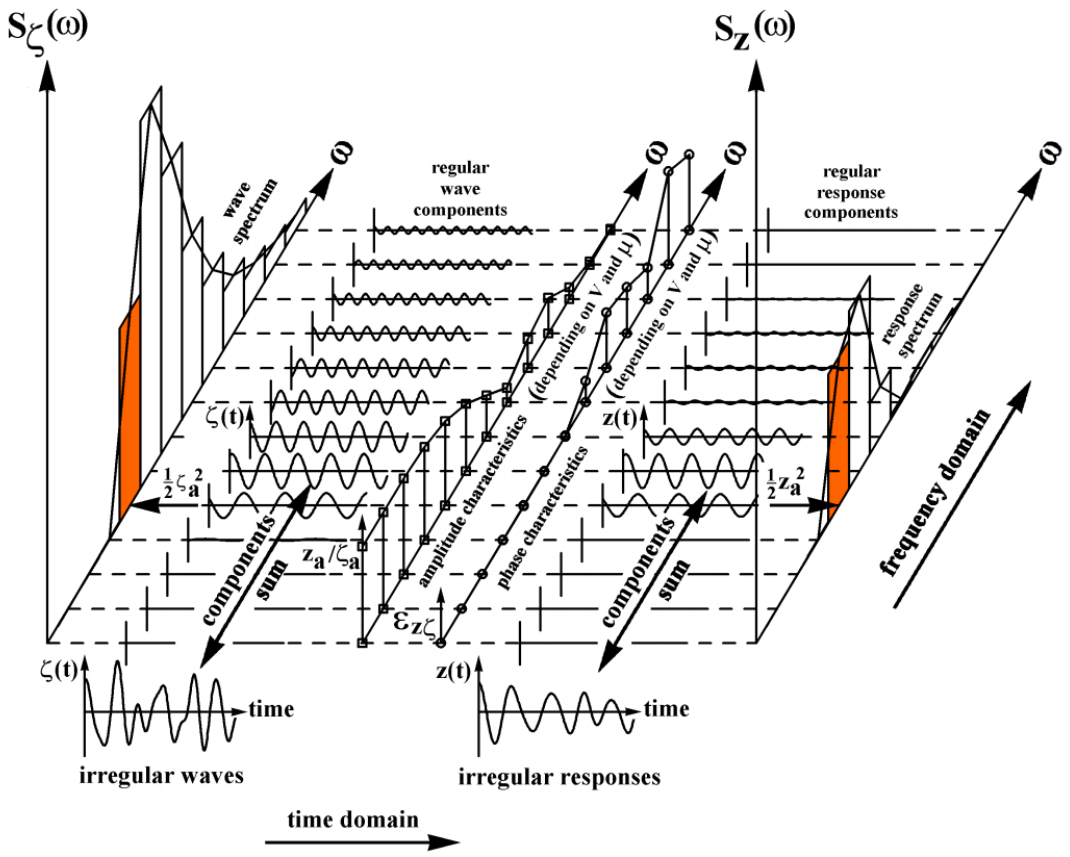

FIGURE 2.7: Method of calculating the body responses from waves.

2.3 Morison Equation

When using the Morison equation, the wave forces are composed by adding up the drag and inertia loads of the structure. The equation is applicable, when the drag is significant. This is mostly the case when the structure is relatively small compared to the wavelength. The rule of thumb is $D/\lambda < 0.2$. Here D is the (equivalent) diameter of the structure in meters. The Morison equation can be expressed as follows:

$$F = \rho_w C_m V \dot{u} + \frac{1}{2}\rho_w C_d A u|u| \tag{2.26}$$

in which:

ρ_w	=	Density of seawater = 1025 [kg/m^3]
V_r	=	Reference volume [m^3]
C_m	=	Inertia coefficient [-]
C_d	=	Drag coefficient[-]
u	=	Flow velocity in direction of the considered force [m/s]
$\dot{u}$	=	Flow acceleration in direction of the considered force [m/s] [m/s^2]
A	=	Projected area normal to the flow direction [m^2]

The inertia coefficient is related to the added mass coefficient by $C_m = 1 + C_a$. The added mass coefficient and the drag coefficient of the structure is determined by the geometrical shape and roughness. For this study, the coefficient are determined with help of [15].

Chapter 3

Environmental data collection

(Confidential)

Chapter 4

Design Basis

(Confidential)

Part 1: Concept Study

Chapter 5

Concept screening

In this chapter, several new concepts are envisaged. The concepts are ideated by means of individual thinking and group brainstorm sessions. The brainstorm sessions are organised with the research and development team of Boskalis and with the client team of Heinrich Hirdes.

5.1 Ideation Approach

Initially, all the ideas envisaged by the contributors of the brainstorm sessions and individuals are listed. During this stage, it is important to go for quantity, thereby making sure that the the production of concepts is divergent. Furthermore, criticism of ideas generated should be discouraged. By suspending judgment, participants will feel free to generate unusual out-of-the-box ideas. In the second stage, ideas are combined and clustered to obtain new ideas. Ideas that are clearly non-feasible are removed for the ideas list. The ideas are also checked with the initial design requirements. The ones that do not fit the design requirements are removed. Current chapter focuses on the concept ideas that remained after this stage. In the last stage, ideas are checked on different criteria with the help of a multi-criteria analysis. During this stage, the most promising idea or ideas are chosen. This stage is elaborated further in chapter 6.

For the generation of concepts, a systematic approach is used by combining existing components or ideas into a new concept for the removal of munitions. Also some out-of-the box ideas are envisaged, although most of the time these ideas were considered non-feasible because of its long development time or high costs and are therefore not mentioned in current work.

All the envisaged ideas belong to a certain common basic concept;

- Seabed-based (section 5.2)
- Amphibious (section 5.3)
- Separate crawler-vessel (section 5.4)
- Vessel-based (section 5.5)
- Semi-submersible (section 5.6)

Each basic concept has a number possible variations, which will be elaborated in the following sections. Some of the considered variations are too complex, expensive or impractical. These are removed from the concept analysis. Conclusions regarding the variations that will be taken into account in the multi-criteria analysis are depicted in a box.

5.2 Seabed-based concept

FIGURE 5.1: Trenchformer, tracked submersible vehicle owned by Boskalis.

The seabed-based concept consists of a submersible, remotely-operated crawler. All equipment required to detect and remove munitions (i.e. manipulators, dredge pump, detection coils) is mounted on the crawler. The vehicle is maneuvered over the seabed by means of a locomotion system. The vehicle is non-buoyant, thus situated on the seabed. This way, the vehicle is more stable in harsh environmental conditions than a conventional hovering ROV. During the ideation process, several variations of this concept were identified. The variations are split in two groups; locomotion system and power supply method. These variations are explained in the following subsections. The pros and cons of this concept are listed in table 5.1.

The idea for this concept is derived from existing submersible crawlers. An example is the Trenchformer owned by Boskalis shown in figure 5.1. This large tracked submersible crawler is designed for subsea cable trenching. The two large tracks make it a stable platform for trenching, even on soft soils.

TABLE 5.1: Advantages and disadvantages for the seabed-based concept.

Advantages	**Disadvantages**
• Fixed to the seabed, thus stable platform in waves and current. • Operable over the full range of proposed water depths (1-10 m) • Proven concept in the offshore submersibles industry.	• High financial and engineering investment, based on experience from the Trenchformer. • The mobility of the vehicle in soil-dependent. This could lead to problems when trying to move over boulder fields as defined in chapter 3.

Locomotion system

Several variations of the locomotion of the vehicle are possible. The locomotion system for vehicles moving predominantly on the ground can be classified in the following main classes: tracked, legged and wheeled locomotion. Moreover, there also exist vehicles featuring combinations of these locomotion classes, known as hybrid locomotion. A elaborate review and comparison of different land-based locomotion system can be found in Appendix C.

Examples of different locomotion system are displayed in figure 5.2. Figure 5.2a shows "The Crabster" CR200 robot, a six-legged underwater walking robot for precise inspection and manipulation on the seabed. Figure 5.2b shows the Zebro, a six-legged robot with inherently high mobility. Its independently controlled legs produce special gaits that enhances its rough terrain climbing abilities with minimal operator input. Figure 5.2c shows a vehicle with amphirol locomotion. This system has excellent capability of moving over extremely soft soils, but is inefficient on hard soils.

(A) Legged locomotion: The Crabster. [16]

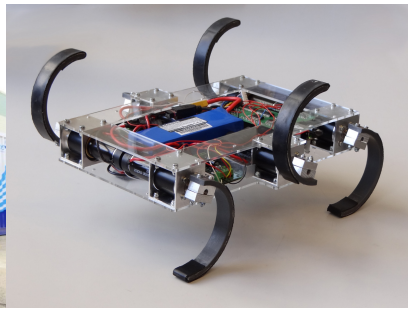

(B) Hybrid wheel-leg locomotion: Zebro developed by TU delft. [17]

(C) A vehicle with an "amphirol" locomotion system

FIGURE 5.2: Examples of crawlers with different locomotion systems.

Conclusion
The comparison conducted in Appendix C shows that a wheeled solution would not have sufficient traction, while legged and hybrid locomotion requires a significant investment and development time. Since this is not desired for current work it can be concluded that the only viable solution for current concept is a tracked locomotion system.

Power supply

The vehicle requires power for the locomotion system and all its tooling, sensors and other equipment required for munitions recovery. An option is to supply power to the vehicle by an umbilical originating from a generator on a nearby support vessel. An example of an application of this method is the Trenchformer by Boskalis shown in figure 5.1. Power supply by umbilical has proven its use in the underwater vehicle industry many times before, mostly for cable trenching purposes. Drawback of an umbilical is that it decreases the maneuverability of the crawler. In strong tidal areas, the current load on the umbilical can become significant.

Another method to supply power is by using a conventional diesel engine but rising the engine components out of the water. An example of this method is displayed in figure 5.3a. The photo shows two elevated excavators, the Starfish I and II, designed by Jan de Nul. These vehicles are adjusted versions of the Hitachi EX 120 ton excavator. The operating depth of the vehicles is limited to six meters. The Starfish I (right of 5.3a) is fixed to its undercarriage by means of a big tube. The Starfish II features a scissor-mechanism, which can adjust the height of the top platform of the vehicle. A clear advantage of the elevated platform solution is that it uses a conventional diesel motor and electronics, making it an cost-efficient solution. Furthermore the maneuverability of the vehicle is unrestricted. Disadvantage is the working depth and workability of the vehicle. The elevated platform makes it subtle to overturning in case of uneven/rough seabed or strong current conditions.

The last considered method of power supply for the seabed based concept is the snorkel engine. The submersible vehicle has an watertight diesel engine and takes in air by means of a snorkel that protrudes above the water surface. Komatsu designed an underwater dozer using this method of powering, displayed in figure 5.3b. The vehicle is capable of underwater operations at a maximum depth of 7 m. The vehicle is remote-controlled giving it unrestricted maneuverability. For this power supply method the working depth and workability of the vehicle are limited, since the protruding snorkel makes it subtle to wave and current loads which could lead to lack of traction or overturning.

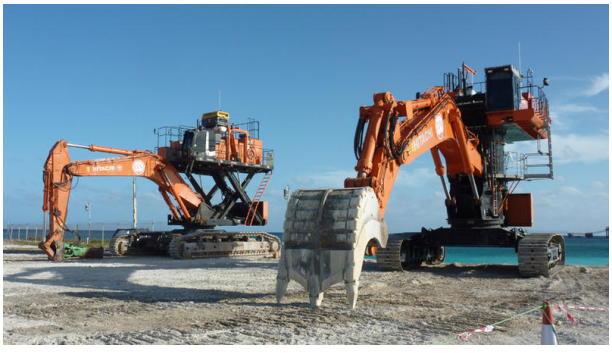

(A) The starfish elevated platform excavators.

(B) The Komatsu underwater dozer with snorkel attachment

FIGURE 5.3: Examples of (semi-)submersible crawlers.

Some unconventional power supplies were also considered, such as solar power, batteries, nuclear power and surface independent diesel engines (closed-loop). However, these solutions where rendered clearly non-feasible because of their lack of technology readiness, high costs or dangers.

Conclusion
Taking the advantages and drawbacks into account, it can be concluded that there is no significant advantageous power supply solution. Therefore all the above options will be taken in consideration in the multi-criteria analysis.

5.3 Amphibious concept

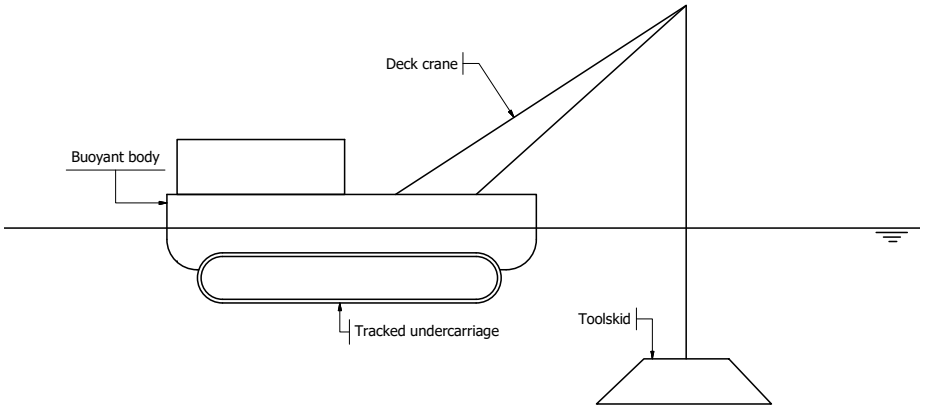

FIGURE 5.4: Layout sketch of the amphibious concept. (Note: the figure displays a single variation of the base concept)

This concept consists of a remote operated munitions toolskid that is deployed by means of an amphibious vessel. When the project area is too shallow a locomotion system will take over the function of mobilizing the vehicle. The vehicle carries a toolskid, which consists of a frame on which all equipment required for the safe removal of munitions is mounted. The skid is lowered to the seabed by a deployment system mounted on the amphibious vessel. A sketch of the concept is displayed in figure 5.4. The pros and cons of this type of concept are listed in table 5.2. The following paragraphs explain the most important variations on the amphibious concept.

TABLE 5.2: Advantages and disadvantages for the amphibious concept.

Advantages	**Disadvantages**
• Operable over the full range of proposed water depths (1-10 m) • Can move quickly over land and water without rearrangements and thus can potentially have a high production.	• Conflicting interest when designing for an hydrodynamic balanced floater which can work in harsh current and waves, and on the other hand a soft terrain crossing vehicle. • Barely used in the offshore industry.

Locomotion system

The possibilities for the locomotion systems of the amphibious concept are similar to those of the seabed-based concept. Refer to section 5.2 for more information on the locomotion systems. For similar reasons as noted in section 5.2 the tracked locomotion system is identified as the most feasible solution for mobilizing the amphibious concept.

Propulsion when floating

When in floatation mode, there a two possible propulsion methods that are considered: self-propelled or towed/pushed by a support vessel. When self-propelled, the vehicle is more agile in maneuvering and positioning. However, the thruster system requires the ability to be remotely-controlled from a distance, since no personnel is allowed on deck during a munitions removal operation. Thus, this would require two self-propelled vehicles; the amphibious vehicle itself and a support vessel from which the amphibian thruster system is controlled. This will results in a higher investment, day-rates and maintenance costs compared to begin towed. Taking this in account, the method of towing/pushing the amphibious vehicle will be more cost-effective.

Conclusion
A towed or pushed vehicle is the most economically viable solution for the propulsion of the amphibious concept compared to self-propelled. Thus, only the self-propelled solution is taken into account in the MCA.

Position keeping method

During the scanning and removing of munition, the vehicle's position and heading needs to be maintained. When on land, the vehicle is moored to the ground by its own weight. When sailing, the concept will require a position keeping method. The methods considered for this study are classified as: anchoring, spud pole system, jack-up system and dynamic positioning.

Anchoring is mechanically the most simple solution. After the anchors are deployed there is no chance of running off position by system failures or blackouts. However, the biggest drawback of anchoring is that it requires handling tugs to position the anchors at the correct location. This increases the operational effort and time significantly. Furthermore dropping the anchor at an unknown location on the seabed in a possible UXO contaminated field could lead to dangerous situations.

Another option is position keeping by spud poles, which is also a low investment solution. An additional advantage is the short setup time compared to anchoring. A drawback of the spud pole systems is the limited maneuverability when the spuds are deployed. Furthermore, the holding capacity of the spuds depend on the soil conditions in the specified area. Two different methods of spuds are possible: gravity spuds and pre-loaded spuds. For convenience, the two methods are combined in the multi-criteria analysis. More information on the difference between these two methods will be discussed in chapter 7.

Another position keeping solution is the jack-up system. The platform will be completely lifted out of the water. Therefore the workability in waves and current for this solution will be high. However, the jack-up is mechanically more complex than spud poles and also requires stable soil conditions. Another drawback is the long time required to jack-up and lower the platform.

Dynamic positioning (DP) has no setup time and will therefore result in the lowest required operational time. The workability of the DP system is independent of the soil conditions and is

not limited by water depth. However, it requires a complex and high-investment thruster and control system. Another drawback of the use of a DP system is that in very shallow water the thrusters will lift soil of the seabed dispense it in the water. This will significantly reduce the visuals during the operation.

Conclusion
Anchoring is a definite no-go, since it can results in dangerous situations when dropping the anchors in a UXO contaminated field. A DP system is also rendered impractical because of its relatively high costs and limited workability in shallow water depths. Taken this in account, it can be concluded that anchoring and DP are not feasible position keeping solutions for current concept. Spud poles and jack-up systems are identified as the most viable solutions and are thus taken in consideration in the multi-criteria analysis.

Toolskid deployment

Two different methods for positioning the toolskid over the target are investigated for current work; deployment by wire rope winches and deployment by an hydraulically controlled rigid arm.

The idea for the first method is to lower the toolskid by wire rope winches and land it on the seabed. This method has the advantage of being mechanically very simple and robust. Subsea lifting by wire rope is frequently used in the offshore industry and well understood. When the toolskid is deployed on the seabed the wire rope is slacked, thus the toolskid motions are uncoupled from the ship motions, making it a stationary and stable platform for munitions recovery. However, the dynamic behaviour during lowering of the deployed object is influenced both by the motion of the vessel and the direct wave loading and current drag load on the object and wire rope. This will create pendulum motions of the skid and could lead to inaccurate landing on the seabed. This can potentially cause hazardous situations when the toolskid touches a suspicious target on landing.

The idea for the second method is to hover the toolskid over the target by means of a rigid hydraulically controlled arm, without touching the seabed. This results in better controllable positioning of the skid . However it also creates an extra demand on the vehicle's/vessel's hydrodynamic stability, since the skid will mostly follow the motions of the vehicle/vessel. Another drawback is the limited working depth of a hydraulic arm compared to deployment by a wire rope.

Conclusion
Taken all the above in account, there is no clear advantageous method yet. The dynamic behaviour of these two methods is completely different (rope vs stiff arm) which makes them hard to compare. Further analysis of both the hydraulic arm and wire rope deployment methods will show which method is best.

5.4 Separate vessel-crawler concept

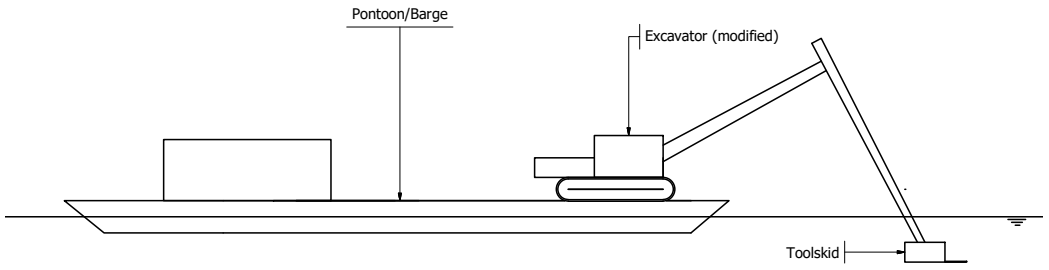

FIGURE 5.5: Layout sketch of the separate crawler-vessel concept. (Note: the figure displays a single variation of the base concept)

An remote-operated crawler crane or excavator carrying a toolskid is placed on a barge or pontoon. When at the desired location, the crawler lowers the toolskid to the seabed. When the water is too shallow for the vessel to operate, the crawler can be deployed from the vessel's deck by means of a deck ramp. A sketch of the concept is displayed in figure 5.5. The pros and cons of this type of concept are listed in table 5.3. The following paragraphs explain the most important variations on separate crawler-vessel concept.

TABLE 5.3: Advantages and disadvantages for the separate crawler-vessel concept

Advantages	**Disadvantages**
• Low investment solution; requires mostly existing and simple components. • Most of the components for this concept are available worldwide (pontoon, excavator/crane) • Operable over the full range of proposed water depths (1-10 m)	• Two separately operated vehicles, thus increased operational complexity. • The vessel requires a sophisticated roll-on/roll-off system to deploy the crawler.

Locomotion system of crawler

The possible locomotion systems for the crawler vehicle are similar than for a seabed-based vehicle. Thus, only a tracked locomotion system is considered for this concept. Refer to section 5.2 for more information on the possible locomotion systems.

Position keeping method

The position keeping methods for this group are similar to those of the amphibious group in section 5.3. This gives two feasible methods: spud pole system or jack-up system.

Propulsion

Also for this group, the vessel can be self-propelled or towed/pushed. Towing/pushing by means of a support vessel is favoured due to its simplicity and low investment, since this method requires only one propelled vehicle (see section 5.3 for more info).

Tool deployment

The methods for toolskid deployment are similar to those of the amphibious concepts. In this case, the hydraulic arm method refers to a vehicle with an hydraulic arm, thus an excavator. The wire rope deployment refers to a mobile crane. For more information on these methods refer to 5.3. Both methods are further analysed for current concept in the multi-criteria analysis.

5.5 Vessel-Based concept

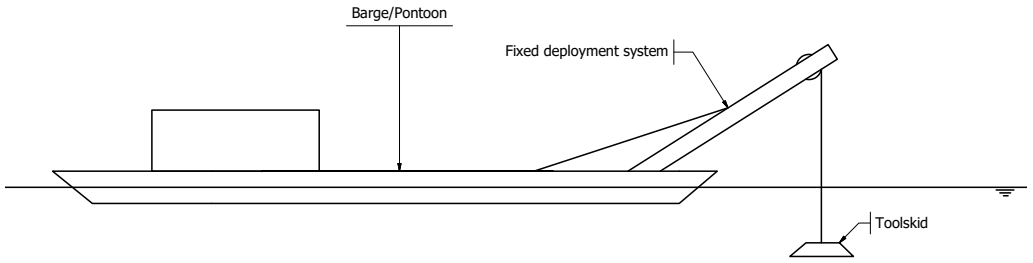

FIGURE 5.6: Layout sketch of the vessel-based concept. (Note: the figure displays a single variation of the base concept)

For this concept, the toolskid is lowered to the seabed by a fixed deployment system mounted on a vessel. The vessel has no ability to move over the seabed and can only position itself by thrusters. Therefore the operational water depth is dictated by the draft of the vessel. A sketch of the concept is displayed in figure 5.6. The pros and cons of this type of concept are listed in table 5.4. A couple of variations on this concept are possible and will be explained in the next paragraphs.

TABLE 5.4: Advantages and disadvantages for the vessel-based concept

Advantages	**Disadvantages**
• Low investment solution. Requires only a barge and a toolskid. • Most components are off-the-shelve available word-wide (pontoon, excavator/crane)	• The operational water depth is limited by draft of the vessel.

Position keeping method

The position keeping methods for this group are similar to those of the amphibious group in section 5.3. This gives two feasible methods: spud pole system or jack-up system.

Propulsion

Also for this group, the vessel can be self-propelled or towed/pushed. Again the towing by means of a support vessel is favoured due to its simplicity and low investment. (see section 5.3 for more info)

Tool deployment

Also the tool deployment options are similar to those of the amphibious concepts. For more information on these methods refer to 5.3. Both tool deployment methods for his concept are taken in consideration for the decision making process.

5.6 Semi-submersible concept

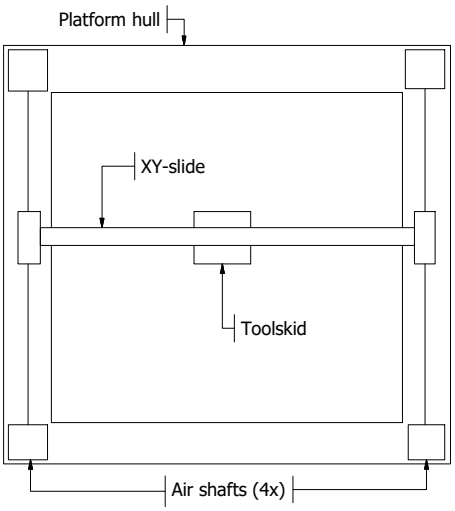

(A) Top view

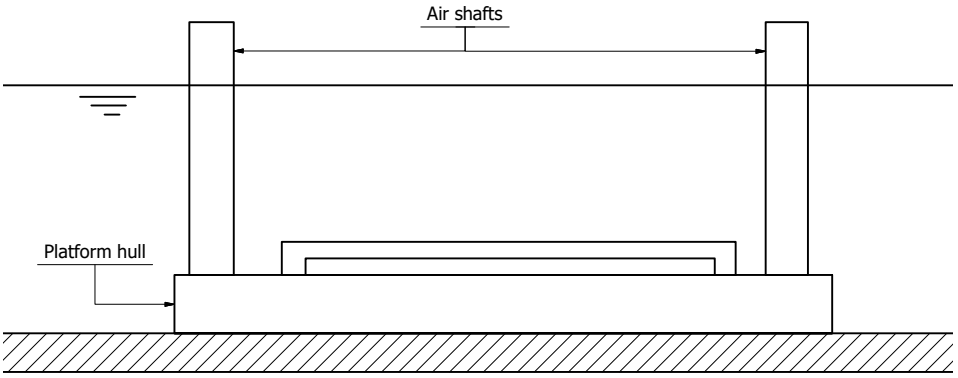

(B) Side view

FIGURE 5.7: Layout sketch of the semi-submersible concept

A remote-operated semi-submersible type structure is outfitted with munitions removal equipment. The equipment is positioned above a large opening in the middle of the platform with the help of a x-y-slide mechanism or similar. The platform can be submersed and landed on the seabed by means of water ballasting. When the ballast tanks need to be emptied, air is supplied by four air shafts at the each corner of the platform. The shafts protrude out of the water at all times. Power for the ballast pumps and munitions removal equipment is supplied by a support vessel. The support vessel pushes or tows the platform to the target location. A concept sketch is displayed in figure 5.7.

Inspiration for this concept are for example the semi-submersibles of Dockwise. Figure 5.8a shows the Dockwise Vanguard, an enormous semi-submersible vessel for transporting oil rigs and other mega-structures. Figure 5.8b shows the NDSQ semi-submersible barge, which is also used for heavy transport but has a much simpler design. The ballast pump can be clearly seen on top of the air shafts.

For this concept, no important variations are identified. The pros and cons of this type of concept are listed in table 5.5.

(A)

(B)

FIGURE 5.8: Pictures of the Vanguard and NDSQ semi-submersible vessel.

TABLE 5.5: Advantages and disadvantages for the semi-submersible concept

Advantages	**Disadvantages**
• Grounded on the seabed during operation, thus stable platform in waves and current. • Simple and cost-effective design.	• The concept requires engineering effort, since it has to be custom built. • The operational water depth is limited by draft of the submersible platform. • The platform has a large footprint on the seabed, inaccurate landing on the seabed could lead to accidentally landing on an UXO.

5.7 Generation of concepts

The next step in to combine the possible variations of the basic concepts to create new solutions for the removal of underwater munitions. Table 5.6 shows a morphological chart which yields a matrix of the concepts and their variations, as defined in previous sections. The generation of concepts is done by choosing a base concept in the first row of the matrix. A new concept can be obtained from the chart by assigning a feasible solution to each of the sub-functions of the concept. As discussed in previous sections, Some of the solutions to sub-functions displayed in table 5.6 are rendered impractical or feasible. These solutions are displayed in grey italic.

In some cases, sub-functions are not applicable to the chosen base concept. For example, if a seabed-based concept is chosen, a propulsion function is not applicable since a seabed-based vehicle will only require a locomotion system to maneuver. Furthermore, the toolskid deployment function is not applicable to the seabed-based vehicle since it does not require a toolskid for the removal of munitions.

TABLE 5.6: Morphological chart of the base concepts with possible variations. (Rejected solutions are displayed in grey italic)

Function	**Solutions**				
Base concept	Seabed-based	Amphibious	Separate crawler & vessel	Vessel-based	Semi-submersible
Locomotion	*Wheeled*	Tracked	*Legged*	*Hybrid*	N/A
Propulsion	Towed / Pushed	*Self-propelled*	N/A		
Power supply	Umbilical	Snorkel engine	Elevated platform engine	Conventional (vessel)engine	
Position keeping	*DP*	*Anchors*	Spuds	Jack-up	By its own weight
Toolskid deployment	By wire-rope	By hydraulic arm	N/A		

After combining each basic concept idea with all possible variations, a total of sixteen feasible concepts are devised:

1 **Seabed-based**

- 1a Submersed tracked crawler with umbilical
- 1b Submersed tracked snorkel crawler
- 1c Submersed tracked elevated platform crawler

2 **Amphibious**

- 2a Tracked amphibian, spud pole system, toolskid deployment by wire rope
- 2b Tracked amphibian, jack-up system, toolskid deployment by wire rope
- 2c Tracked amphibian, spud pole system, toolskid deployment by hydraulic arm
- 2d Tracked amphibian, jack-up system, toolskid deployment by hydraulic arm

3 **Separate crawler-vessel**

- 3a Spud pontoon, toolskid deployment by crane
- 3b Jack-up pontoon, toolskid deployment by crane
- 3c Spud pontoon, toolskid deployment by excavator
- 3d Jack-up pontoon, toolskid deployment by excavator

4 **Vessel-based**

- 4a Spud pontoon, toolskid deployment by wire rope
- 4b Jack-up pontoon, toolskid deployment by wire rope
- 4c Spud pole pontoon, toolskid deployment by hydraulic arm
- 4d Jack-up pontoon, toolskid deployment by hydraulic arm

5 **Semi-submersible**

- 5a Semi-submersible platform

Chapter 6

Concept evaluation

In this chapter the most promising concept(s) from previous chapter is/are determined with help of a multi-criteria analysis (MCA). First, the approach is discussed in section 6.1. The criteria used for the MCA are selected based on the most important performance features that were selected during interviews with all people that will be involved in working with the finalized concept and are listed in section 6.2. Finally, the results and conclusion of the MCA are given in section 6.3 and 6.4.

6.1 Evaluation approach

The concepts from previous chapter are compared to each other by means of a MCA. Multi-criteria analysis establishes preferences between the concepts by reference to a set of objectives that are identified, and for which measurable criteria have been established to assess the extent to which the objectives have been achieved. An MCA offers a number of ways of aggregating the data on individual criteria to provide indicators of the overall performance of certain concepts. MCA techniques commonly apply numerical analysis to a matrix in two stages:

1. Scoring: the expected consequences of each option are assigned a numerical score on a strength of preference scale for each option for each criterion. More preferred options score higher on the scale, and less preferred options score lower. In current study, scales ranging from 0 to 5 are used, where 0 represents a least preferred option, and 5 is associated with a most preferred option. All options considered in the MCA therefore fall between 0 and 5.

2. Weighting: numerical weights are assigned to define, for each criterion, the relative value between the top and bottom of the chosen scale. In case of current study, the scale is 0 - 1.

The total score of each concept are compared to select the most promising concept.

6.2 Criteria selection

The criteria decide on how to compare the contribution of different ideas to meeting the objectives of current study. This requires a selection of criteria to reflect the performance of each concept. Each criterion must be measurable, in the sense that it must be possible to assess, at least in a qualitative sense, how well a particular option is expected to perform in relation to the

criterion. Each criteria is giving a weight based on its importance. This weight is determined during several meetings with operators and experts on current munitions removal tools. The importance or weight of each criteria is determined by assigning it a mark from 0 to 10. The weight is than obtained by normalizing the mark. The next paragraphs give a description of the criteria used for the MCA in this study.

Productivity; Defines how many targets can be recovered in a certain time span. Important things to keep in mind are the transit time between targets and the time it takes to scan, free, remove and store objects.

Operational complexity; Defines the complexity of a typical operation during a project. Import aspects that are considered are the number of separately controlled vehicles or vessels, required personnel and the number of actions required to obtain the desired operational result i.e. removal of the target.

Workability; Defines the ability to operate the tool in a sea state with waves, currents and wind velocities.

Robustness; Defines the degree to which a system operates correctly and is reliable in the presence of exceptional inputs or stressful environmental conditions, but also the reliability during normal conditions. Import aspects that are considered are the probability of failure of certain components, the consequences of this failure and the complexity of a recovery of the concept after failure.

Area coverage; Defines the ability to use the tools in confined and shallow water areas, as defined in chapter 3.

Feasibility; Defines the resources required to fabricate and the expected success of the proposed tool. Important aspects that belong to this criteria are technology readiness, required development time and technical complexity of the envisaged concept. Also the availability of the materials required for the concept are taken into account.

Costs; Defines the overall capital and operational expenditures of the tool.

6.3 Multi-criteria analysis results

(Confidential)

6.3.1 Sensitivity analysis

(Confidential)

6.4 Conclusion

(Confidential)

Chapter 7

Conceptual layout

(Confidential)

Part 2: Proof of Concept - Workability

Chapter 8

Workability analysis approach

The workability of the concept is identified as the most important aspect influencing the feasibility and performance of the proposed concept. Specifically, the horizontal and vertical motions of the toolskid attached at the end of the excavator are assumed to be the most critical. Therefore the remaining part of this study is dedicated to determining the operational limits for which the motions of the skid are within the limit as will be defined in section 8.1. The model that is used to check the limiting criterion is defined in 8.3.

8.1 Limiting criteria

(Confidential)

8.2 Physical parameters

For the motion analysis carried out in current study, only the cyclic motions of the toolskid are important. Thus, only the motions due to wave action is investigated. The current and wind load on the structures are assumed constant, and will therefore only lead to static offset. A range of physical parameters is used as input in the model to obtain an estimate of the maximum motions for all possible sea states. The range of parameters used in current thesis is noted in table 8.1. The parameters are chosen based on the expected environmental conditions that are found in coastal and confined waters.

Table 8.1: Physical parameters ranges used in the workability analysis.

Variable		**Range**	**Step size**
Significant wave height	H_s	0.50 - 1.50 [m]	0.25
Peak wave period	T_p	2 - 8 [s]	1
Wave direction		0^o - 360^o	15
Water depth	d	2, 5, 10 [m]	-

8.3 Sources of motion

The proposed concept consist of many components from which motion can originate. The following list discusses all the identified sources of motion in a top-down order (starting from

the toolskid) and discuss why - or why not the source is taken into account in the workability analysis.

1. **Wave-induced bending of the excavator arm.** Due to the long arm of the extended boom and stick, the wave load can cause high bending moments, and thus a significant motion response in the tip of the excavator. The motion due to bending is taken into consideration in the workability analysis in chapter 9.

2. **Excavator backlash mobilization due to tolerances.** There will be cyclic wave loading of the excavator arm whereby the backlash in the different joints will be constantly mobilized. Due to the long arm of the excavator, even small tolerances can cause significant motions of the excavator tip. This source is described in chapter 9.

3. **Hogging and sagging of the pontoon.** (i.e bending of the ship's hull due to waves). Assumed to be negligible compared to other motion sources, since the wave action in shallow and confined water is benign. This source can become significant for high sea states ($H_s > 2$ m) .

4. **Wave induced motions of the pontoon.** This is identified as one of the main sources of motion and is thus taken in consideration in chapter 10.

5. **Spud system backlash mobilization due to tolerances**. Also the spuds and spud keepers have certain tolerances incorporated in their design. However, this problem can be easily solved by using an hydraulic clamp on deck which maintains a constant horizontal load on the spuds, hereby eliminating the mobilisation of the tolerances. This system is mimicked from the *Aeolus* jack-up vessel [18]. Thus, no further analysis of the backlash in the spuds system is carried out.

6. **Spud-seabed interaction**. It is expected that the spuds are not actually fixed on the seabed, but can move laterally and vertically due to soil shearing. However, to reduce the extent of current study, the motion due to spud-soil interaction is neglected. The motions due to this sources are assumed to be negligible compared to other sources.

The items that are taken into account in the workability model of current study are underlined.

8.4 Motion amplitude

For each of the motion sources of previous section which are considered for current study, a maximum motion amplitude of the excavator tip is calculated. The total amplitude is then determined by summing the motion amplitude of each individual source. This is expressed as follows:

$$w^e = w_t + w_d + w_p \tag{8.1}$$

in which w^e is the total motion amplitude in m and w_t, w_d and w_p are respectively the maximum motion amplitudes due to excavator backlash mobilisation, excavator arm bending deflection

and pontoon motions in m. These motion amplitudes are in turn the resultant of the motion amplitude in x,y and z-direction. For example, the maximum motion amplitude due to backlash mobilization is expressed as:

$$w_t = \sqrt{x_{a,t}^2 + y_{a,t}^2 + z_{a,t}^2} \tag{8.2}$$

in which $x_{a,t}$, $y_{a,t}$ and $z_{a,t}$ are the motion amplitudes in x, y and z direction due to backlash mobilization in m.

Chapter 9

Excavator motion analysis

Considering only the excavator, the motions of the tip have two causes: mechanical backlash mobilisation and arm deflection due to wave loading. The next two sections show how these are modelled and calculated in current study. The results of the model are discussed in 9.3.

9.1 Mechanical backlash

Backlash is defined as the maximum distance or angle through which mechanical connections can move with applying small force. The force on the boom and stick due to wave loading is cyclic. In this study, it is assumed that the hinges and connection are constantly moving over their clearance distance in order to determine a conservative estimate of the motions. The motion amplitude is determined by a tolerance stack up, defined as the amount that parts can move at assembly due to the clearance between the assembly's internal features such as holes and external features such as a fasteners.

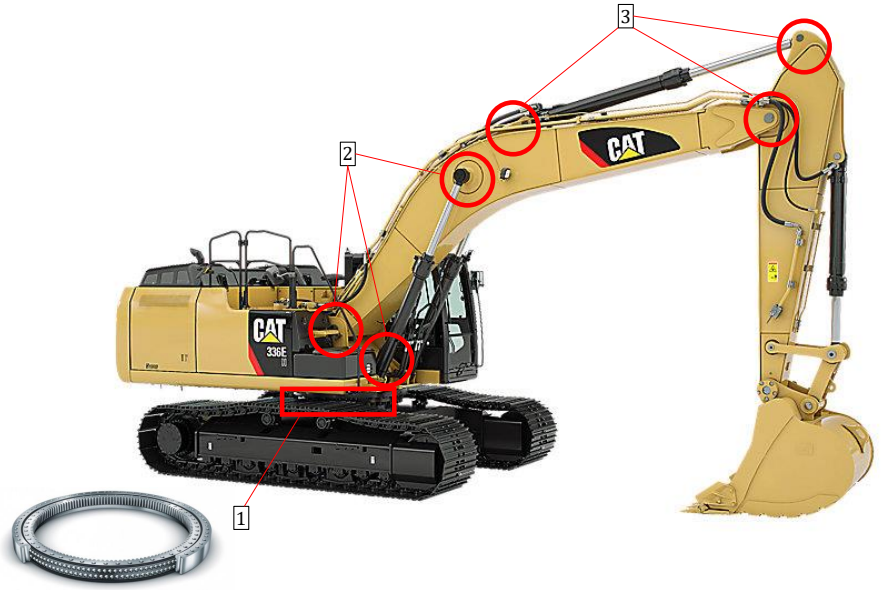

FIGURE 9.1: Overview of the joints with tolerances resulting in an excavator tip offset.

For current study, the worst case tolerance stack-up method is used [19]. This method assumes that all dimensions in the tolerance stack-up may be at their worst-case maximum or minimum, regardless of the improbability. The backlash due to tolerance stack-up in two different planes

are estimated: x-y-plane and x-z-plane. The main sources of mechanical backlash which are analysed are displayed in figure 9.1 and consist of:

1. **Swing bearing, connecting the excavator base to the undercarriage**. The tolerance of the swing bearing is specified by the manufacturer as a given tilting clearance and a tolerance in the gear system. The dimensions of the swing bearing are estimated by help of excavator drawings.
2. **Pin-shaft and bush joints connecting the boom to the base and hydraulic cylinders.** The tolerances of the pin-shaft joints are determined by the ISO 258 guideline for joint tolerances [20]. This guideline specifies the maximum allowable clearance between pin and shaft as they leave the factory.
3. **Pin-shaft and bush joints connecting the stick to the boom and hydraulic cylinders.** Determined by the ISO 258 guideline [20].

9.1.1 Assumptions

In order to simplify the backlash mobilisation model, a couple of assumptions are required. The following is assumed in this study:

- It is assumed that the motion amplitude due to backlash mobilisation is independent of the wave load or direction, since the backlash is mobilized by applying small force.
- To incorporate the change of tolerance due to wear or changing temperature, the tolerances are multiplied by a factor of safety of 1.5 [19].
- The boom and stick are assumed to have no weight and no friction in the joints. Thus the joints are free to move in any direction.
- The analyzed backlash is assumed to work in only one plane at a time. Thus, the maximum motion amplitude is defined as the maximum value of the motion in x-y-plane and x-z-plane.

9.1.2 Tolerance Analysis: X-Y-plane

The backlash in the x-y-plane is determined by the rotation around the z-axis of the excavator swing, boom and stick due to tolerances in these components. A schematic of the components with an exaggerated rotation is displayed in figure 9.2. The sources which result in a angle of rotation are numbered. Each source results in a certain angle of rotation. The results are given in table 9.1.

The maximum attainable rotation of the boom or stick due to tolerances of a single joint and the corresponding offset of the tip is given in table 9.1. An elaboration of the way of calculating this rotation is given in Appendix G. The total offset of the tip of the excavator due to assembly rotation is calculated by:

$$w_t = (\theta_b)\frac{2\pi \cdot a_b}{360} + (\theta_b + \theta_s)\frac{2\pi \cdot a_s}{360} \tag{9.1}$$

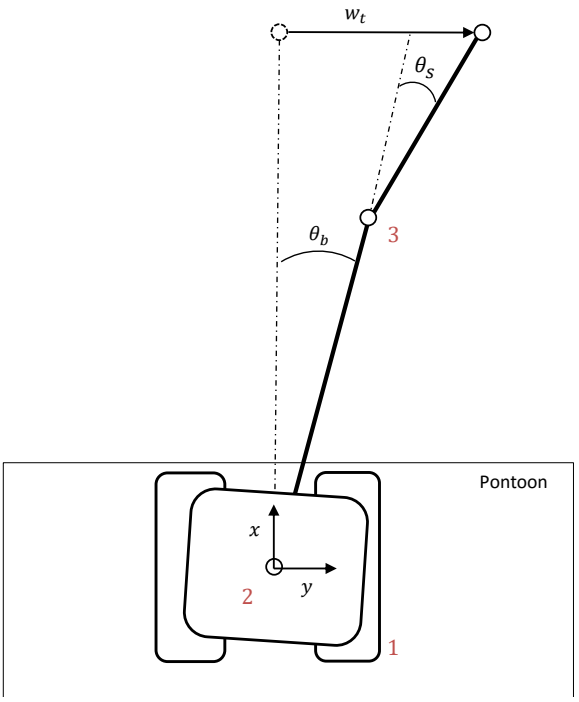

FIGURE 9.2: Schematic overview of the rotations in the x-y-plane due to tolerances. The desired position of the excavator arm is represented by the dotted lines.

in which:

θ_b = Maximum rotation of the boom due to tolerances
θ_s = Maximum rotation of the stick due to tolerances
a_b = Arm of the boom (determined in chapter 7) = 10 [m]
a_s = Arm of the stick (determined in chapter 7) = 8.2 [m]

TABLE 9.1: Rotations of the excavator arm due to tolerances and the resulting tip offset in the x-y-plane.

Source #	Description	Max. angle [deg]	Tip offset [cm]	Rotator
1	Swing bearing gear	±0.026	±0.8	Boom
2	Pin-shaft joint, base-boom	±0.118	±3.7	Boom
3	Pin-shaft joint, boom-stick	±0.119	±1.8	Stick
	Total tip offset (worst case)	w_t	±6.3 [cm]	

9.1.3 Tolerance Analysis: X-Z-plane

In the x-z-plane, the backlash mobilisation results from the rotation of the boom and stick around the y-axis due to the tolerances in different components. A schematic of this plane is displayed in figure 9.3. The results of the tolerance analysis is summarized in table 9.2. The total offset and the direction of the tip of the excavator due to assembly shift in this plane is

dependent on the angle of the boom and stick with respect to each other and the excavator base. For this simplified case, it is assumed that the tip can move in a circle with a radius w_t calculated by equation (9.1) and depicted in figure 9.3. An elaboration of the way of calculating the rotation given in the table is given in Appendix G.

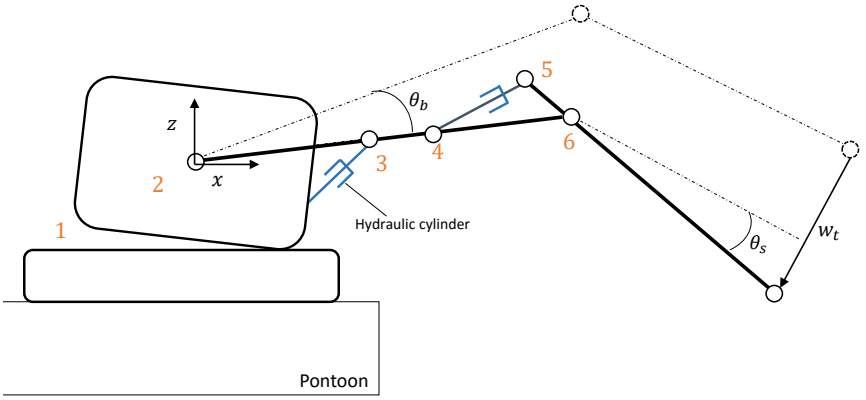

FIGURE 9.3: Schematic overview of the rotations in the x-y-plane due to tolerances. The desired position of the excavator arm is represented by the dotted lines.

TABLE 9.2: Rotations of the excavator arm due to tolerances and the resulting tip offset in the x-z-plane.

Source #	Description	Max. angle [deg]	Tip offset [cm]	Rotator
1	Swing bearing tilt clearance	±0.084	±2.4	Boom
2	Pin-shaft joint, base-boom	±0.028	±0.6	Boom
3	Pin-shaft joint, boom-cylinder	±0.024	±0.5	Boom
4	Pin-shaft joint, boom-cylinder	±0.040	±0.6	Stick
5	Pin-shaft joint, cylinder-stick	±0.040	±0.6	Stick
6	Pin-shaft joint, boom-stick	±0.035	±0.5	Stick
	Excavator tip offset (worst case)	w_t	±5.0 [cm]	

The excavator tip ofset due to backlash mobilization in the X-Y-plane has the highest value. Thus, for the remainder of the study the tip motion amplitude due backlash w_t **= 6.3 cm.**. This amplitude is independent of the wave load and direction.

9.2 Excavator Arm Bending

Another cause of dynamic movement of the excavator tip is the deflection of the boom and stick due to cyclic wave loading. The following paragraphs discuss the steps taken to determine the magnitude of the deflection due to bending.

9.2.1 Assumptions

The following assumptions apply to this section:

- The boom and stick are treated as two separate cantilever beams.
- The geometry of the excavator arm is complex. To obtain an estimate of the deflection, a simplified rectangular tube model is used. The boom and stick assumed to have equal cross sections, and the cross sectional area is constant over the length. Specifications and a schematic of the geometry can be found in Appendix E.
- Current loads and wind loads on the excavator arm are neglected since the current and wind velocity is assumed constant in time. Therefore these loads will only lead to static bending of the excavator arm, thus not important for the dynamic analysis considered in this study.
- The tip of the boom is assumed to be loaded by the reaction forces and moment at the fixed end of the cantilever beam of the stick (see figure 9.4).
- To simplify the calculation and obtain a worst case scenario, the stick is assumed to be always perpendicular to the flow (see figure 9.4).

9.2.2 Deflection model

As explained, the boom and stick are modelled as two separate cantilevers. The two cantilever models are displayed in figure 9.4 for two different wave directions. The deflection of the tip of the excavator arm is calculated with Euler-Bernoulli beam equation [21] expressed as:

$$EI\frac{d^4\delta}{dx^4} = q(x) \tag{9.2}$$

in which

E = Young's modulus, assumed constant over length of the beam [Pa]
I = Second moment of area, assumed constant over length of the beam [m^4]
x = horizontal position on the beam
δ = Deflection of the beam in z-direction [m]

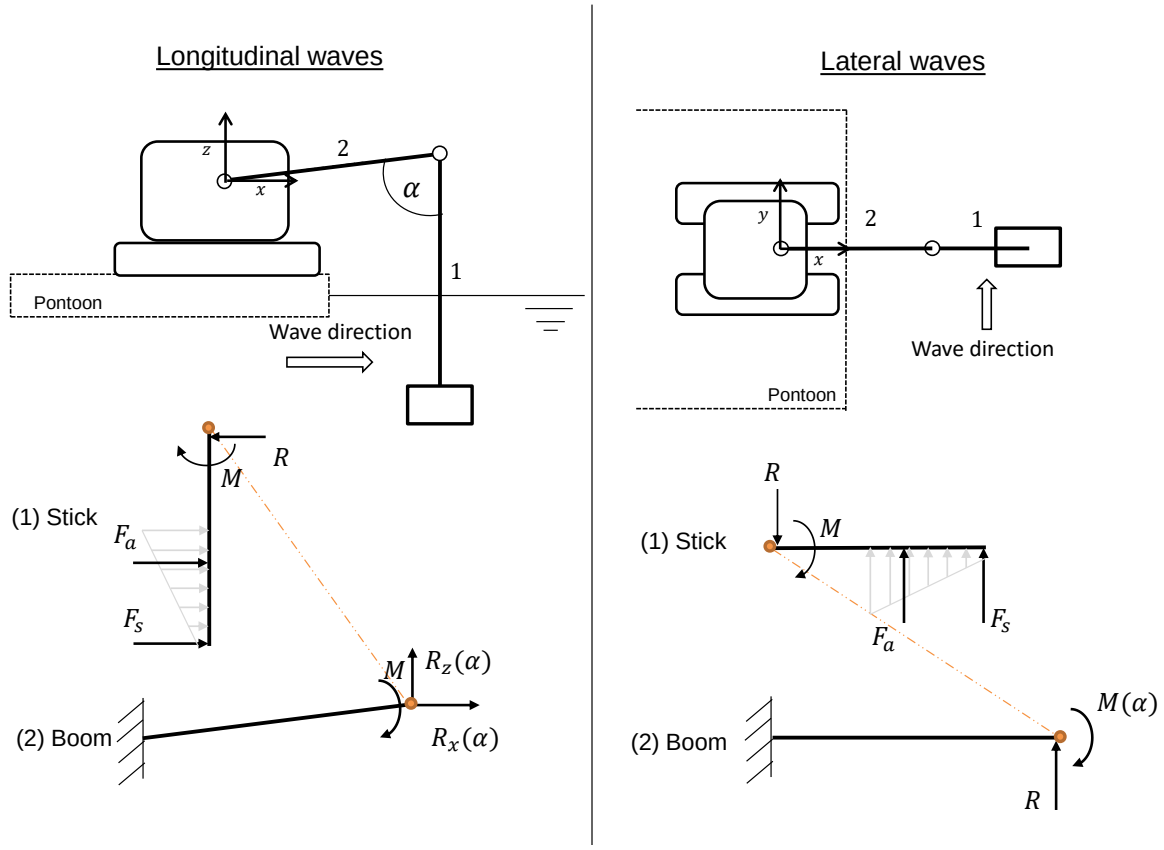

FIGURE 9.4: Schematic overview of the cantilever model used to calculate the bending of the excavator arm. Left: case for head and following waves. Right: case for beam waves

For a cantilever the boundary conditions at the fixed end are: $w|_{x=0} = 0$; $\frac{dw}{dx}|_{x=0} = 0$ and at the free end are determined by the applied forces and moment. Solving eq. (9.2) for these boundary conditions gives an expression for the deflection at the tip of the cantilever due to point loads and moments:

$$\delta = \sum_{i=1}^{n} \left(\frac{F_i x_i^2}{6EI} (3L_b - x_i) \right) + \frac{ML_b^2}{2EI} \tag{9.3}$$

where

F_i	=	Point load i at position x perpendicular to the beam [N]
n	=	Number of point loads [-]
x_i	=	Horizontal position of the point load i on the beam [m]
L_b	=	Length of the beam [m]
M	=	Applied moment on the beam [N/m]

The maximum deflection of the tip of the excavator is the sum of the deflection of the two cantilevers due to the wave loads discussed in the following subsection. When the loads are

known, the total dynamic deflection of the beam is calculated as:

$$\delta_{tot} = \delta_b + \delta_s \tag{9.4}$$

Where δ_b and δ_s are the maximum deflections of the respectively the boom and stick calculated with (9.3). The maximum motion amplitude due to bending of the arm is than equal to the total deflection, i.e. $w_d = \delta_{tot}$.

9.2.3 Wave loads

The wave loads are split in two components; the wave load on the toolskid F_s and the wave load on the excavator arm F_a as depicted in figure 9.4. The characteristic length of the toolskid and the arm are much smaller than the considered wave lengths (i.e. $D \leq 0.2\lambda$), thus the Morison equation is applied.

Wave load on toolskid F_s
Using the Morison equation given in (2.26), the wave load on the toolskid can be expressed as:

$$F_s(t) = \rho_w V_t C_m \dot{u}(t) + \frac{1}{2}\rho_w C_d S u(t)|u(t)| \tag{9.5}$$

in which:

ρ_w	=	Density of seawater = 1025 [kg/m^3]
V_t	=	Reference volume of the toolskid estimated at 1 [m^3]
C_m	=	Inertia coefficient of the toolskid [-]
C_d	=	Drag coefficient of the toolskid [-]
$u(t)$	=	Horizontal wave particle velocity, time dependent [m/s]
$\dot{u}(t)$	=	Horizontal wave particle acceleration, time dependent [m/s^2]
S_t	=	Projected area of the toolskid normal to the force direction [m^2]

The horizontal wave particle velocity is calculated with equation (2.1). To obtain the maximum horizontal particle velocity amplitude in a certain sea state (for a given H_s and T_p), the wave elevation amplitude is determined by (2.7). The guideline for a conservative drag coefficient for a typical complex subsea structure in oscillatory flow is given in [15] as $C_d = 2.5$. The inertia coefficient of the toolskid is estimated at $C_m = 2.5$, following the guideline for a box shaped structure [15]. The projected area of the toolskid is estimated from the preliminary design of the toolskid shown in figure (confidential). In longitudinal direction $S_t = (h_s \cdot b_s) = 1.0 \cdot 1.4 = 1.4$ m^2 and in lateral direction $S_t = (h_s \cdot l_s) = 1.4 \cdot 1.2 = 1.68$ m^2

Wave load on excavator arm F_a

The sectional drag force on the excavator arm is calculated by using the Morison equation:

$$f_a(z,t) = \rho_w A_r C_m \cdot \dot{v}(z,t) + \frac{1}{2}\rho_w C_d S_a \cdot v(z,t)|v(t)| \tag{9.6}$$

where:

z = vertical distance from the still water level downwards [m]
A_r = Reference cross sectional area of the beam, for rectangular $A_r = \pi \cdot a^2$ [m^2], where $a = \frac{1}{2}$ width of the beam. [15]

The drag coefficient for the excavator arm is derived from a rectangular cylinder [15], $C_d = 2$. The inertia coefficient is determined for a similar shape, $C_m = 1.5$.

The total load on the arm is determined by integrating equation (9.6) over the submerged part of the stick:

$$F_a(t) = \int_0^{L_s} \left(\rho_w A_r C_m \cdot \dot{u}(t) + \frac{1}{2}\rho_w C_d S_a \cdot u(t)|u(t)| \right) dz \tag{9.7}$$

This load is distributed over the submerged length of the excavator arm. Figure 9.5 shows a graph of the sectional wave load on the excavator arm (in steps of 0.1 m). It shows that the load distribution is roughly quadratic. Thus, an equivalent point load of the distributed load is assumed to work at $\frac{1}{3}$ of the length of the stick below the still water line. Since the stick is assumed to be perpendicular to the still water surface, the wave lift and downward load is assumed to be negligible compared to horizontal wave load.

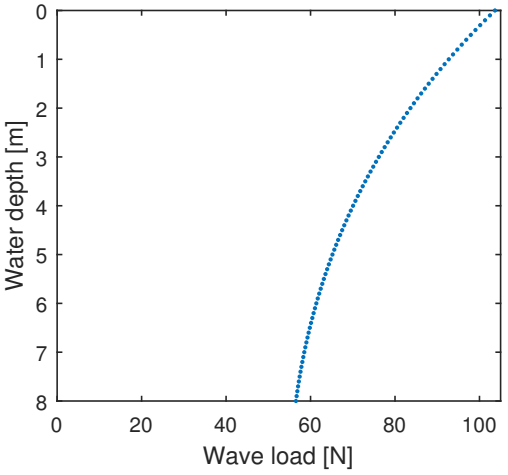

FIGURE 9.5: Graph showing the distribution of wave load on the excavator arm.

9.2.4 Offset

Both loads are schematically shown in figure 9.4. As discussed earlier the total tip offset due to bending of the excavator arm is determined by equation (9.4). The offset of the stick can now

be determined by combining (9.3), (9.5) and (9.7):

$$\delta_s(t) = \frac{F_a(t)l_a^2}{6EI}(3l_s - l_a) + \frac{F_s(t)l_s^3}{3EI} \tag{9.8}$$

in which l_a is the arm length of the wave load on the excavator stick and l_s is the length of the stick in m. This expression is equal for both following and beam waves as shown in figure 9.4. The expression for the deflection of the boom is different, depending on the angle between the boom and stick α. In the case of beam waves, the reaction force on the boom is in pure y-direction, while in the case of following waves, the reaction force on the boom is decomposed in a x- and z-component. Furthermore, the reacting moment on the stick in beam waves is decomposed in a torsion moment and bending moment, depending on the angle α. While in the case of following waves, the reacting moment is pure bending. For following waves the expression for the deflection of the boom is:

$$\delta_{b1}(t) = \frac{R_z(\alpha, t)l_b^3}{3EI} + \frac{M(t)l_b^2}{2EI} \tag{9.9}$$

For beam waves the expression for the deflection of the boom is:

$$\delta_{b2}(t) = \frac{R(t)l_b^3}{3EI} + \frac{M(\alpha, t)l_b^2}{2EI} \tag{9.10}$$

To obtain the overall maximum amplitude, the Morison equations are calculated in the time domain while varying the angle between the boom and stick α. A graph of the maximum motion amplitude due to bending is given in the following section for varying wave directions.

9.3 Results

Before the results of the discussed models are shown, a definition of the wave direction relative to the pontoon is given in figure 9.6. Following waves are noted by a direction of 0°. Head on waves are noted by a direction of 180°. Note that this definition applies to all the polar graphs in current study.

The horizontal and vertical motion amplitude of the excavator tip due to backlash is determined in section 9.1. It is assumed that this amplitude is independent of environmental conditions, and thus has an equal value for each wave direction and sea state. The maximum value of the two cases is used, which is estimated to be 6.3 cm. A polar plot of the amplitude due to backlash is shown in 9.7.

In contrary to the motions due to backlash, the motions due to arm deflection are highly dependent on the sea state. For current study, the beam deflection response is based on regular shallow water waves. The response is calculated for multiple sea states and water depth combinations. The maximum value over all water depths is plotted in figure 9.8. It shows the maximum deflection of the tip for a number of wave directions, wave periods and a significant wave height of H_s=1 m. To make it comparable with other graphs, the radial range of the graph

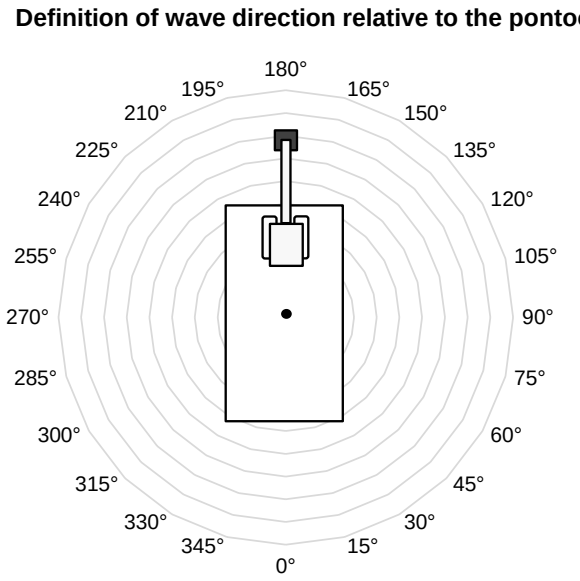

FIGURE 9.6: Definition of the wave direction relative to the pontoon.

is equal to the graph of the backlash. For a better view, a zoomed version of the graph can be found in Appendix H. The graphs shows that the effect of bending on the motion amplitude is highest for beams waves. In this direction the excavator arm is less stiff. (Note: in the the case of excavator arm bending, the motion amplitude are not linear, since the non-linear Morison equation is used to obtain the wave loads.)

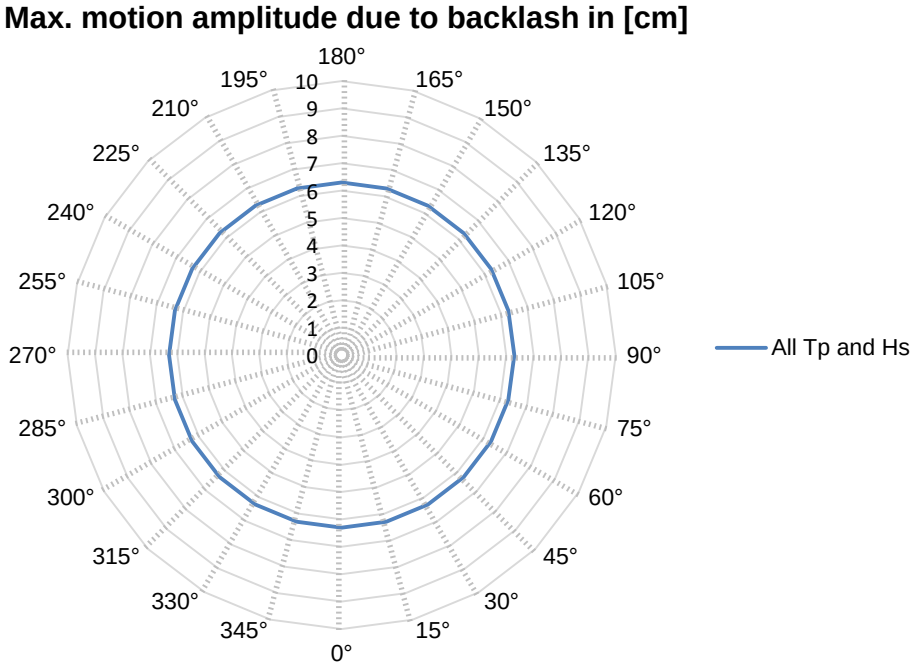

FIGURE 9.7: Motion amplitude of the excavator tip due to backlash.

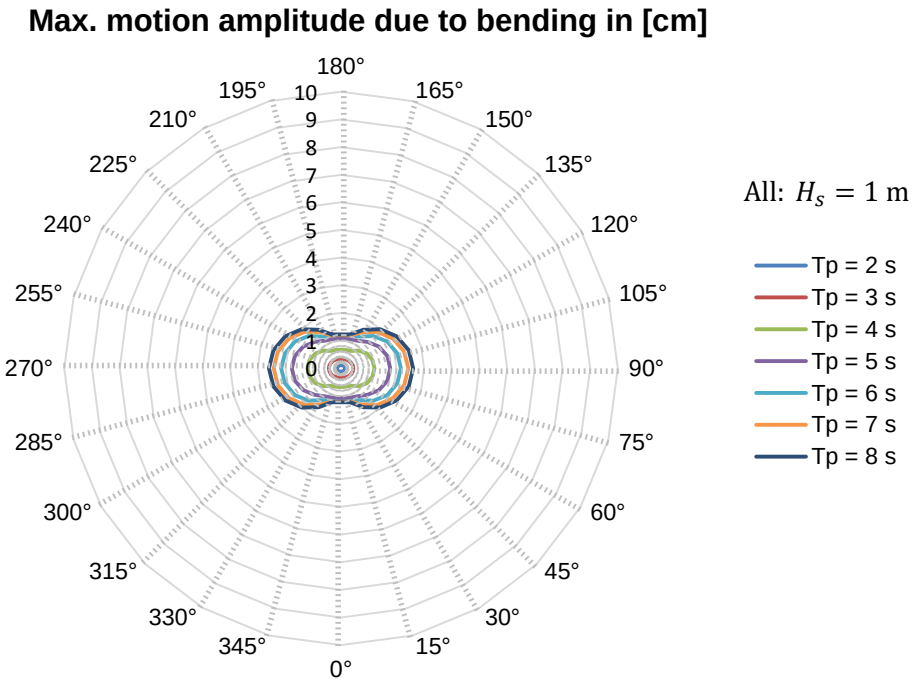

FIGURE 9.8: Motion amplitude of the excavator tip due to bending.

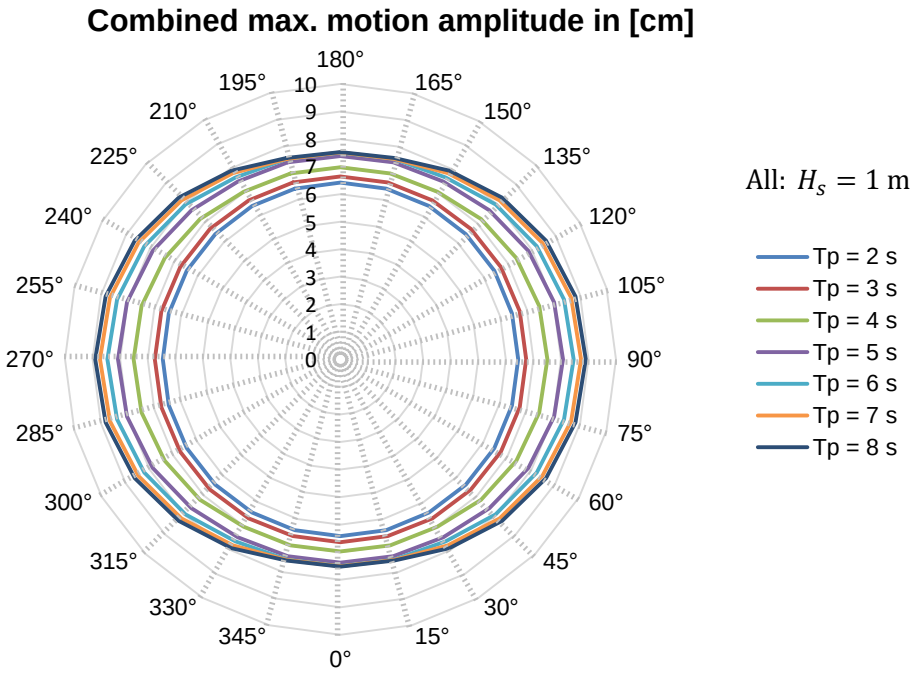

FIGURE 9.9: Motion amplitude of the excavator tip due to combined arm bending and tolerance mobilisation.

9.4 Conclusive remarks

(Confidential)

Chapter 10

Moored vessel motion analysis

The purpose of this part of the study is to identify the motions of the excavator tip due to wave loading on the pontoon when moored. The method of modelling the pontoon and mooring configurations in AQWA is explained in section 10.1. The results of the motions analysis is discussed in 10.2. Conclusive remarks concerning the moored vessel motions are given in 10.3

10.1 Moored vessel models

The following paragraphs define the pontoon and mooring models as used in *Ansys AQWA*. All the models are based on the same basic pontoon of which the characteristics and hydrostatics are defined in chapter 7. First, a free-floating model is conceived, used as a basis for comparison with other models. Three different mooring system are observed in current study; gravity spuds, backhoe puds (i.e. pre-loaded spuds), and a jack-up system. The first two are modelled in AQWA. The jack-up system is not implemented, since for this study the jack-up is assumed to have no wave-induced motions when in jack-up mode.

10.1.1 Base model: Free-floating pontoon

The base model consists of a free-floating pontoon as displayed in figure 10.1. Note that this model is not a feasible solution for the proposed concept, since the pontoon will not be able to maintain its position without a mooring system. The results of the motion analysis of this model is used as a basis for comparison with the moored pontoon models.

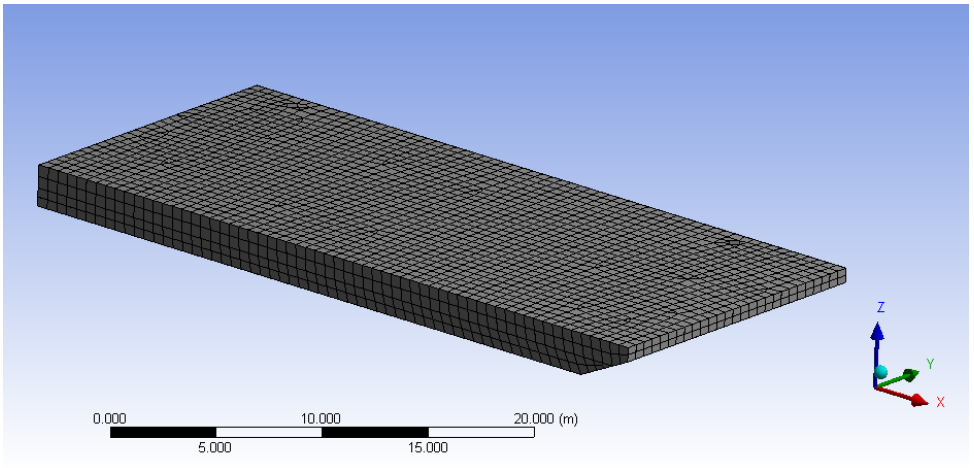

FIGURE 10.1: Screendump of the *E801* pontoon panel mesh in AQWA.

10.1.2 Model 1: Gravity spuds mooring

The first moored pontoon model consists of the basic pontoon outfitted with two gravity spuds on the port side of the pontoon. A deck layout of the pontoon with spuds is shown in figure (confidential). In AQWA the spuds are modelled as springs, located at the position where the spuds would penetrate the seabed. A schematic side view of the model is shown in figure 10.2.

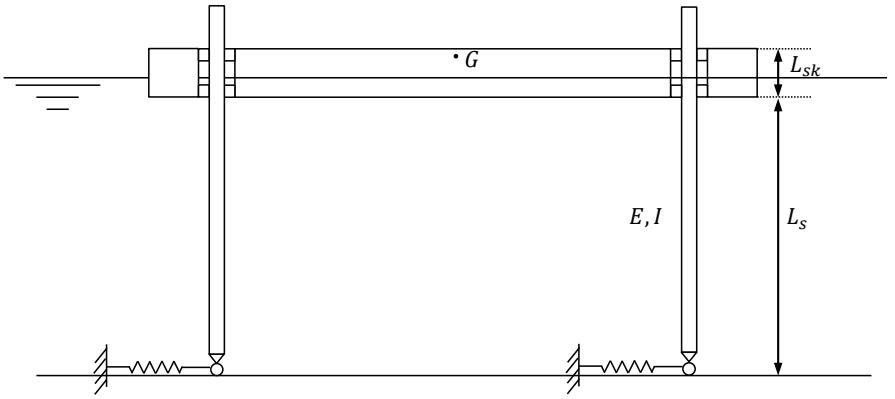

FIGURE 10.2: Model of the pontoon with gravity spuds.

According to [22], the spud end acts as a ball-joint at the seabed. The pontoon plus the spuds are thus modelled as one rigid body, free to rotate around the connection point of the spuds to the seabed. This model is implemented into AQWA by giving the pontoon an additional stiffness matrix relative to the center of gravity of the vessel. When a rigid body is supported by a set of translational springs relative to a defined point as depicted in figure 10.3, the stiffness matrix of the spuds is expressed as [23]:

$$K_s = \begin{bmatrix} nk_x & 0 & 0 & 0 & k_x \sum c_i & -k_x \sum b_i \\ & nk_y & 0 & -k_y \sum c_i & 0 & k_y \sum a_i \\ & & nk_z & k_z \sum b_i & -k_z \sum a_i & 0 \\ & & & k_z \sum {b_i}^2 + k_y \sum {c_i}^2 & -k_z \sum a_i b_i & -k_y \sum a_i c_i \\ & & & & k_z \sum {a_i}^2 + k_x \sum {c_i}^2 & -k_x \sum b_i c_i \\ \text{(symm)} & & & & & k_y \sum {a_i}^2 + k_x \sum {b_i}^2 \end{bmatrix} \tag{10.1}$$

in which:

n	=	Number of spuds
k	=	Stiffness of the spud in x,y or z-direction [N/m]
a_i, b_i, c_i	=	Position vector from the center of gravity of the pontoon for spud i [m]

In figure 10.3 points p_i define the locations where the springs are connected to the spuds. For current model, two connection points are used: p_1 and p_2. For the case of gravity spuds, the stiffness of the vertical springs $k_z = 0$, since the pontoon can move freely in vertical direction and the friction between the spuds and spud keepers is neglected. Also the pontoon is free to

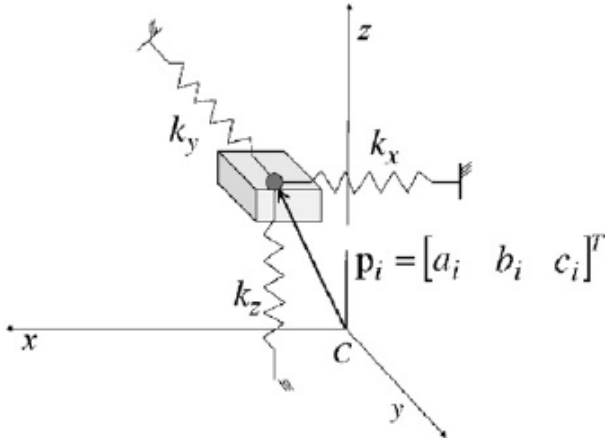

FIGURE 10.3: Rigid body supported by a set of translational springs.

pitch. Thus every heave and pitch component in equation (10.1) is set to zero. Furthermore, it is assumed that each spud is symmetrical and thus have equal stiffness in x- and y- direction. This simplifies equation (10.1) for the considered gravity spuds model to:

$$K_{s,1} = \begin{bmatrix} nk_h & 0 & 0 & 0 & 0 & -k_h \sum b_i \\ & nk_h & 0 & -k_h \sum c_i & 0 & k_h \sum a_i \\ & & 0 & 0 & 0 & 0 \\ & & & k_h \sum {c_i}^2 & 0 & -k_h \sum a_i c_i \\ & & & & 0 & -k_h \sum b_i c_i \\ (\text{symm}) & & & & & k_h \sum {a_i}^2 + k_h \sum {b_i}^2 \end{bmatrix} \tag{10.2}$$

in which k_h is the stiffness of the spuds in horizontal direction. The horizontal stiffness of the spuds is determined by the geometrical and physical properties of the spuds and pontoon. A simple cantilever model is used to obtain the magnitude of the stiffness. An expression used to determine the horizontal stiffness using equation (9.2) is:

$$k_h = \frac{3EI_h}{L_s^2 \cdot (L_s + L_{sk})} \tag{10.3}$$

where:

E	=	Young's modulus of the spuds [N/m^2]
I_h	=	Moment of inertia of the spuds around the horizontal axis [m^4]
L_s	=	Length of the free end of the spuds as displayed in figure 10.2 [m]
L_{sk}	=	Length from the top to the bottom spudkeeper as displayed in figure 10.2 [m]

For a circular spud the moment of inertia around the horizontal axis is expressed as:

$$I_h = \pi \cdot \frac{(D_o)^4 - (D_i)^4}{64} \tag{10.4}$$

where:

D_o = Outer diameter of the spuds [m]
D_i = Inner diameter of the spuds [m]

For an overview of the input parameters used for this model, refer to Appendix I.

10.1.3 Model 2: Backhoe type mooring

The second model consists of the basic pontoon, outfitted with a spud system mimicked from the *Koura* backhoe dredger of Boskalis (figure 10.4). The spud system of the *Koura* is chosen because its hull has roughly the same dimensions as the pontoon chosen in this study. During operation the spuds system is able to lift the pontoon slightly out of the water with help of winches, thereby increasing the anchorage and making it less sensible to waves by fixing the pontoon to the spuds.

FIGURE 10.4: Photo of the *Koura* backhoe dredger.

For this spud system model, an additional stiffness matrix is added to equation of motion of the pontoon. The stiffness in vertical direction is dominated by the softest spring, which are the cables lifting the pontoon out of the water depicted in red in figure 10.5. The total stiffness in vertical direction of a single spud is expressed as:

$$k_z = \frac{N_w A_w E}{L_w} \tag{10.5}$$

in which:

N_w = Number of wires connecting the spud to the pontoon, for current study $N_w = 4$
A_w = Nominal cross sectional area of the wire [m^2]
E = Young's modulus of the wire [N/m^2]
L_w = Length of the wire (depicted in figure 10.5) [m]

The horizontal stiffness of the spuds is calculated by means of equation (10.3). Since the spuds of the *Koura* are geometrically complex due to stiffeners and side plates, the horizontal moment of inertia I_h is given an empirically determined value defined in the specification sheet of the

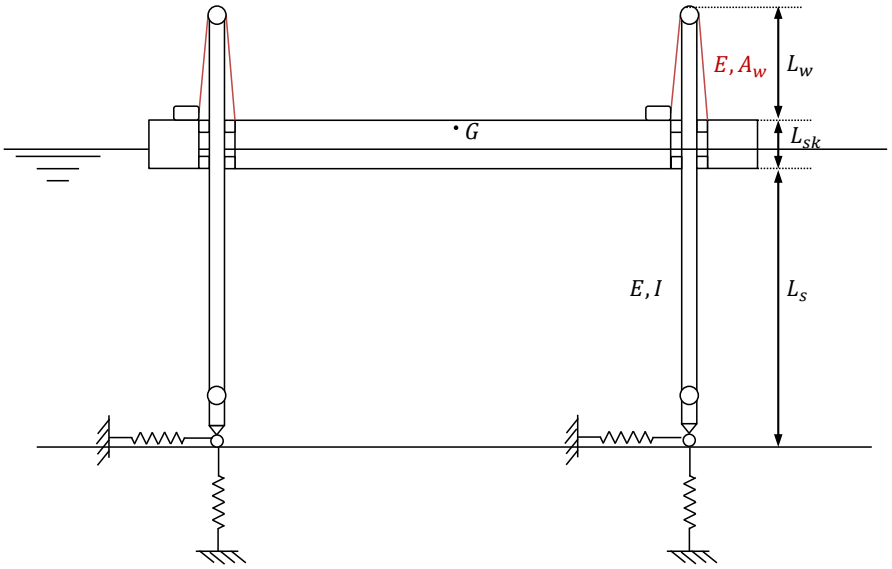

FIGURE 10.5: Model of the pontoon with backhoe type spuds.

backhoe pontoon [24]. For an overview of the input parameters used for this model, refer to Appendix I.

10.1.4 Model 3: Jack-up system

The dynamic motion of a pontoon lifted out of the water by a jack-up system is assumed to be negligible compared to the motions due to excavator arm discussed in previous chapter. Therefore the diffraction analysis for the jack-up is omitted and the wave induced motions of this model are not assessed.

10.2 Results

The models discussed in previous section are simulated in Ansys AQWA to obtain the motion response in the frequency domain. The graphs shown in this section are all calculated for a significant wave height of $H_s = 1$ [m]. Since linear wave theory is assumed, these results can easily be transformed to other significant wave heights by multiplying the motion amplitude value with the desired H_s. All the graphs shown in this section are the resulting motions of the x-,y- and z-direction. For graphs showing the motion amplitude decomposed in x-, y-, and z-direction, refer to Appendix H.

Figure 10.6 and 10.7 show the motion response of the excavator tip for the free-floating and gravity spuds model for $H_s = 1$. A zoom of the graph showing the smaller wave periods is depicted in figure 10.8.

Figure 10.9 shows the motions for the backhoe spuds model. For all wave directions, the motion amplitudes have a maximum value of 8 cm. The graph shows the largest motion amplitude for quartering waves(135° and 225°), and the smallest amplitude for following waves (0°).

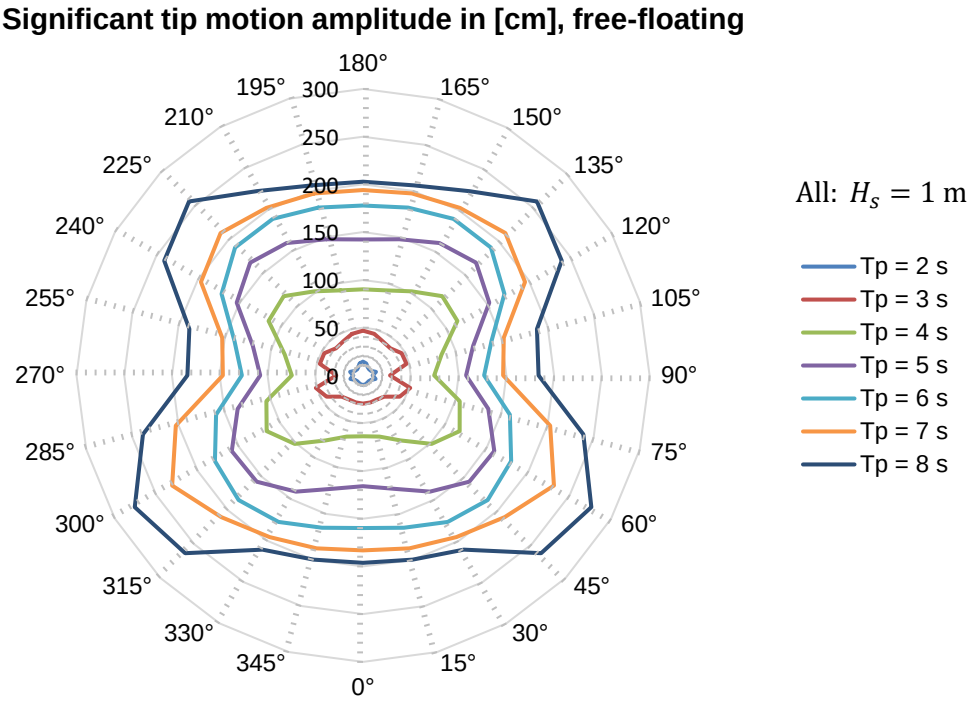

FIGURE 10.6: Motion amplitude of the free-floating model. (Wave direction relative to the pontoon according to figure 9.6)

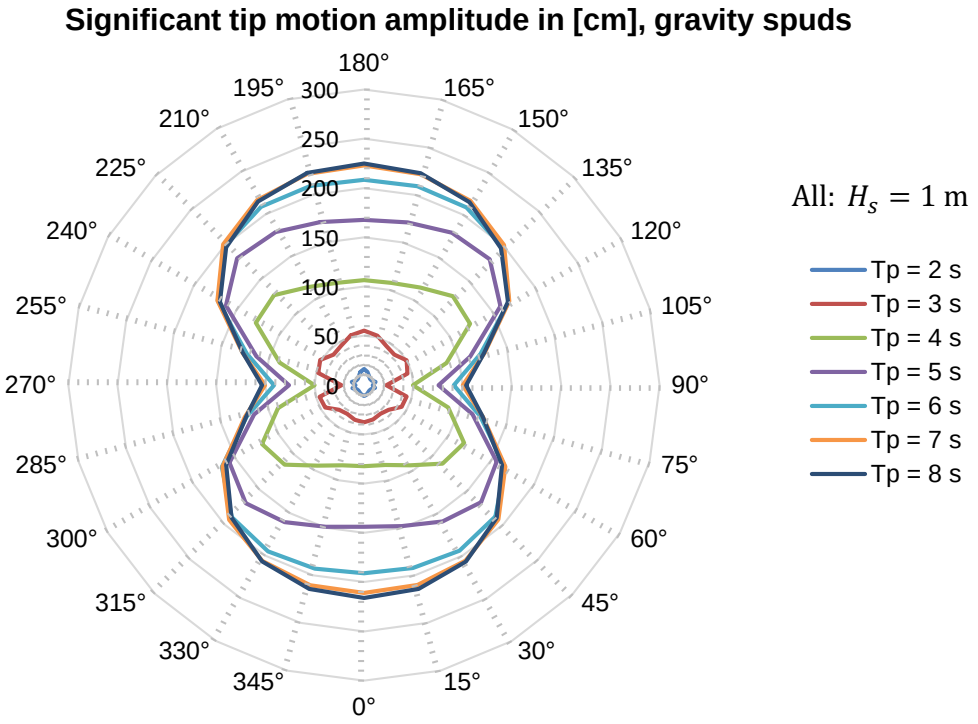

FIGURE 10.7: Motion amplitude of the gravity spuds model. (Wave direction relative to the pontoon according to figure 9.6)

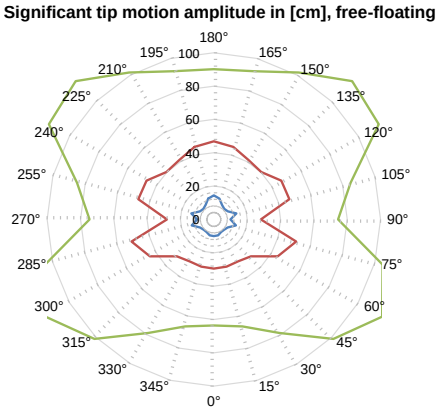

(A) Free-floating model.

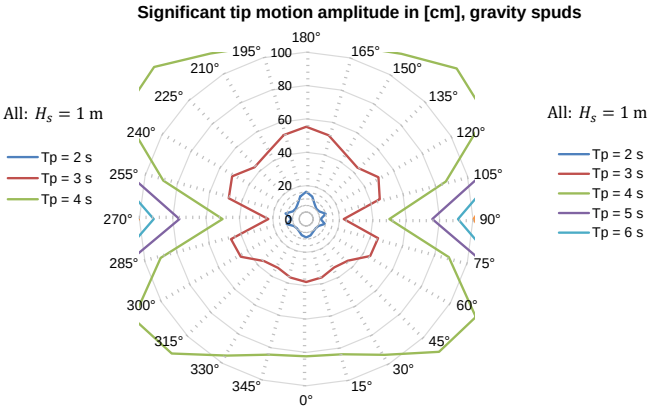

(B) Gravity spuds model.

FIGURE 10.8: Zoomed: motion amplitude of the free-floating and gravity spuds model.

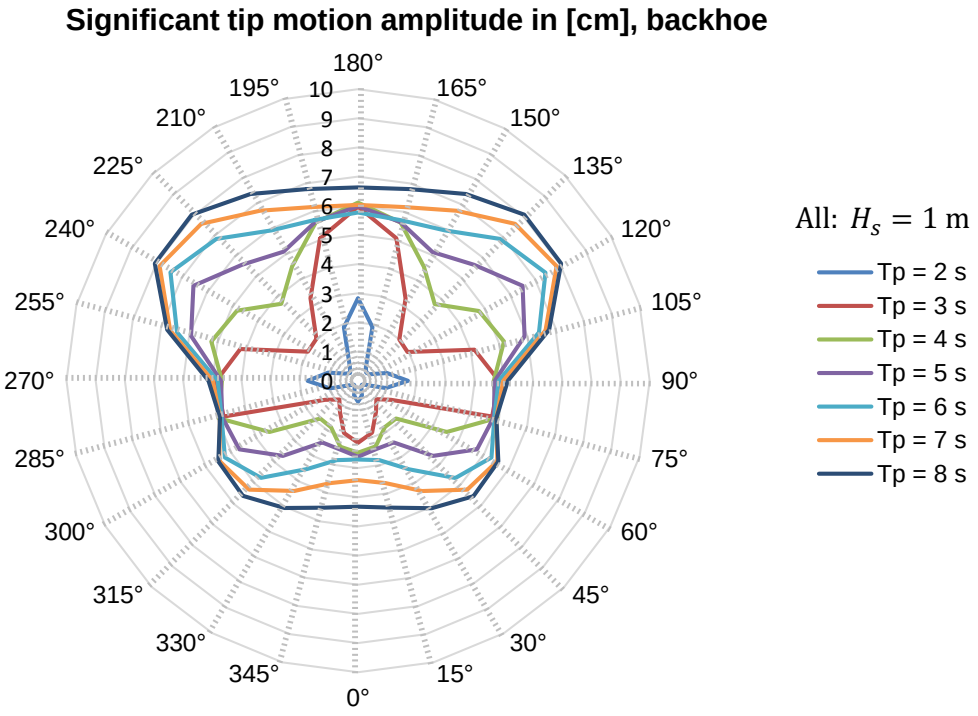

FIGURE 10.9: Motion amplitude of the backhoe spuds model. (Wave direction relative to the pontoon according to figure 9.6)

10.3 Conclusive remarks

(Confidential)

Chapter 11

Workability assessment

(Confidential)

Chapter 12

Conclusions and Recommendations

(Confidential)

Bibliography

[1] Peterson H. Wo überall noch Munition unter Wasser lagert. http://www.welt.de/reise/deutschland/article147871469/Wo-ueberall-noch-Munition-unter-Wasser-lagert.html, October 2015.

[2] Gazzo A. Offshore wind in Europe / Walking the tightrope to success, May 2015.

[3] Holm C. Dangerous Depths: German Waters Teeming with WWII Munitions. http://www.spiegel.de/international/germany/dangers-of-unexploded-wwii-munitions-in-north-and-baltic-seas-a-893113.html, April 2013.

[4] Beddington J. and A. Kinloch. Munitions Dumped at Sea: A Literature Review, January 2005.

[5] Koschinski S. The Old Mine And The Sea: Munitions Cleanup as Opportunity for World-wide Economic Stimulus with Ecological Benefit. *Chemical Weapons Convention*, April 2013.

[6] Geosoft. Success stories. http://www.geosoft.com/resources/success-stories, January 2008.

[7] Itrc. Geophysical Classification for Munitions Response. http://itrcweb.org/GuidanceDocuments/GCMR-1.pdf, October 2012.

[8] GapGeo. Gap Explosive Ordnance Detection UltraTEM. http://www.gapgeo.com/divisions/gap-eod/, 2015.

[9] Smith M. Calls to honour inventor of bomb disposal device. *The Telegraph*, April 2001.

[10] Hornyak T. Army ROV clears underwater ordnance off hawaii. http://www.cnet.com/news/army-rov-clears-underwater-ordnance-off-hawaii/, August 2011.

[11] McDonald J. R. Efficient Shallow Underwater UXO Retrieval. *ESTCP*, August 2009.

[12] Journee J.M.J. and Massie W.W. *Offshore Hydromechanics*. Delft University of Technology, 2001.

[13] Boskalis. Internal communication - Hydrodynamics department.

[14] Hazewinkel M. *Green Formulas*. Springer, 2001.

[15] Det Norske Veritas. Modelling and Analysis of Marine Operations. *DNV-RP-H103*, April 2011.

[16] Jun B.H., Shim H., Kim B., Park J.Y., Baek H., Lee P.M., Kim W.J., and Park Y.S. Preliminary design of the multi-legged underwater walking cr200. *Proc. of the IEEE/OES Oceans*, 2012.

[17] Lopes G.A.D., Babuska R., De Schutter B., and van den Boom A.J.J. Switching max-plus models for legged locomotion. *Proc. of IEEE*, pages 221–226, December 2009.

[18] Boskalis. Internal communication - Aeolus.

[19] Fischer B.R. *Mechanical Tolerance Stackup and Analysis*. CRC Press, 2004.

[20] International Organization for Standardization. ISO 286-2 Round bar and hole tolerances.

[21] Gere J.M. and Timoschenko S.P. *Mechanics of Materials*. PWS Publishing Company, 1997.

[22] Wichers J. and Claessens E.J. Prediction Downtime of Dredges Operating in the Open Sea. *WEDA Conference*, 2000.

[23] Jang S. and Choi Y. Geometrical design method of multi-degree-of-freedom dynamic vibration absorbers. *Journal of Sound and Vibration*, June 2007.

[24] Boskalis. Internal Report; Mooring force analysis.

Appendix A

Additional environmental data

(Confidential)

Appendix B

Types of UXO

(Confidential)

Appendix C

Locomotion systems

The design of the locomotion systems of mobile robots for unstructured environments is generally complex, particularly when they are required to move on uneven or soft terrains, or to climb obstacles, which are all found in the subsea environment for which the tool is designed. In this appendix, a comparative study of the different types of locomotion is discussed.

C.1 Classification

The main classes of ground locomotion are vehicles having tracks, wheels or legs. A combination of these system is also possible (hybrid).

Wheeled
In general, wheeled robots have a higher power efficiency and are faster than other locomotion mechanisms with minimal control effort and mechanical complexity. But their capability of crossing obstacles and moving over soft soil is limited. Since most seabed environments have areas of soft soil and obstacles, wheels are generally not applied for subsea vehicles. Also in the case of the proposed tool, the wheeled class will not be applied.

Tracked
Tracked vehicles have a large ground contact surface, making this system ideal for moving over soft soil. Tracks are also very capable over overcoming obstacles. The power efficiency is fairly good, but move more slowly and consume more energy than wheeled vehicles. Some examples of tracked vehicles used in the offshore industry are shown in figure C.1 To improve the movement over uneven terrain and obstacle crossing, more than two tracks with relative passive mobility can be used. An example of a subsea vehicle with more than two tracks is the Hi-traq by IHC. If the mobility of the tracks is active, the tracks are considered articulated and the vehicle is a tracked-legged hybrid.

Legged
Legged vehicles have the highest mobility of all the locomotion systems. Their obstacles and uneven terrain crossing are superior. However, their capability of walking on soft soils is limited due to the small ground contact surface. Also, the power efficiency is low and they move slow. The system requires complex mechanical components and controls.Two categories can be defined, static or dynamic vehicles. Vehicles that use static movement are always balanced, their center of gravity is always within their ground contact base. Dynamic walking is characterized in that the robot is not always in balance. Many robots that use dynamic walking are continually "falling" and are much more energy efficient, but require a more complex control system. One example of a subsea application with a legged vehicle is 'The Crabster' developed at the Korean

FIGURE C.1: Examples of tracked vehicles: Left-upper: Trenchformer, Boskalis. Right-upper: ROV with track system. Lower: Hi-traq, IHC

Institute of Ocean Science and Technology shown in figure C.2. The robot is used for seabed exploration. Another example of a legged vehicle is the RHex, developed by a consortium of six American and Canadian universities (figure C.2). The Zebro is based on the foundations of the RHex and is developed by TU Delft(figure C.2). These robots have a simple control system and mechanical components while maintaining high obstacle and uneven seabed crossing capabilities.

Hybrid

Hybrid vehicles combine the advantages of locomotion systems, which makes these vehicles very interesting. 3 different hybrid classes are possible; track-leg (TL), wheel-leg (WL), leg-track (LT), wheel-track-leg (WTL). Some examples of hybrid vehicles are shown in figure C.3. These examples are all land based, hybrid vehicles are not applied yet in the subsea environment, however some are made waterproof.

FIGURE C.2: Examples of legged vehicles. Upper: The Crabster. Lower: Rhex and Zebro

FIGURE C.3: Examples of hybrid vehicles

C.2 Comparison

The criteria used for comparison are split in two parts: the criteria that apply to the movement-seabed interaction and the remaining criteria. The score for behavior in current & waves is not yet completed, since this is not known and further assessed. Since movement on the seabed by wheels is limited or impossible because of the in general soft soils, all locomotion categories containing wheels are not considered, but are added to the table for completeness. Furthermore, the dynamic gait legged vehicles category is not considered, since this technology is not even fully understood for land-based robots. Non-considered system are marked grey in the table.

Locomotion ▶ / Feature ▼	Wheeled	Tracked		Legged		WT hybrid	WL hybrid	TL hybrid	WTL hybrid
		2 tracks	4+ tracks	Static	Dyna-mic				
Capability of moving over soft seabed	--	++	++	-	--	+	-	+	+
Capability of moving over uneven seabed	-	+/-	+	++	++	+/-	+	++	++
Obstacle crossing capability	-	+/-	+	++	++	+/-	+	++	++
Slope climbing capability	-	+	+	+	+	+	+	+	+
Speed	++	+	+	--	+/-	+/-	--	+/-	+
Power efficiency	++	+/-	+/-	--	+/-	+/-	--	+/-	+/-
Maneuvering / Steering	+	-	+	++	+	-	+	+	+
Mechanical system simplicity	++	+	+/-	-	-	+/-	-	-	--
Control system simplicity	++	++	+	+/-	--	+/-	-	-	-
Technology readiness (for subsea)	++	++	+/-	-	--	+/-	--	--	--
Behavior in current & waves		TBD	TBD	TBD	--*			TBD	
Costs (++ = lowest cost)	++	+	+/-	-	--	+	+/-	-	-

Appendix D

Feasibility study of crane deployment

(Confidential)

Appendix E

Geometrical properties of the excavator

The table and figure below list the simplified geometrical characteristics of the excavator as used in the model of chapter 8. All the geometric are based on the *Komatsu PC360LC-10*. For a reasonable estimation, it is assumed that the cross section of the boom is equal to the cross section of the stick.

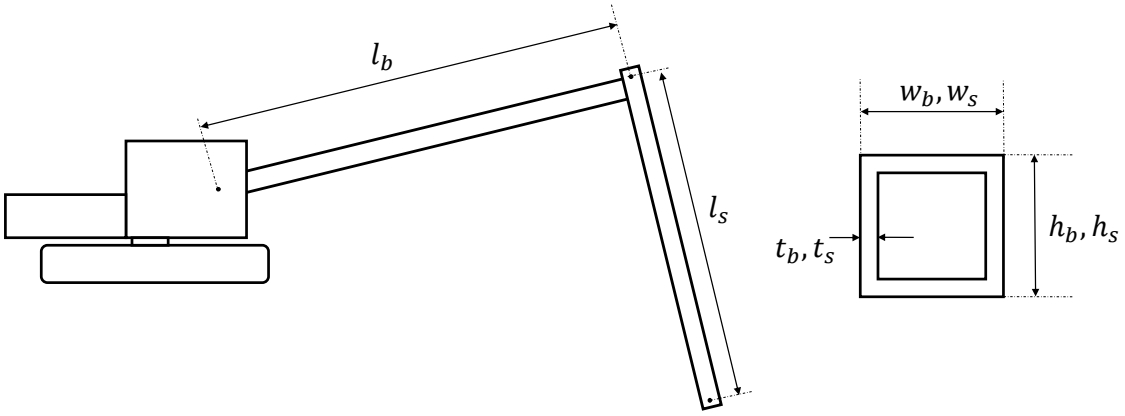

Table E.1: Specification of the excavator.

Description	Symbol	Value	Unit
Width boom	w_b	0.4 [a]	[m]
Height boom	h_b	0.5 [a]	[m]
Thickness boom	t_b	0.0.02 [a]	[m]
Length boom	l_b	10 [a]	[m]
Width stick	w_b	0.4 [a]	[m]
Height stick	h_b	0.5 [a]	[m]
Thickness stick	t_b	0.02 [a]	[m]
Length stick	l_b	8.2 [a]	[m]
E-modulus	E	200 [b]	[GPa]

[a] Estimation based on the specification sheet of the Komatsu excavator defined in chapter 6
[b] Based on A36 structural steel

Appendix F

Pontoon characteristics

The hydrostatics calculated are based on the weight distribution given in the table and figure on the next page. Each component is given a simplified box shape with certain volume in space, by giving it a start and end coordinate in x, y and z-direction. The ballast tanks (BT) are also shown in the figure. In current model, ballast tank 4 and 5 are filled, to obtain the optimal hydrostatic balance.

The center of gravity of the pontoon is also determined from the weight distribution. For the model used in this study, the coordinates of the CoG (relative to the origin point in the figure below) are:

	x	y	z
Center of gravity	18.05 [m]	0.23 [m]	1.34 [m]

	X1 [m]	X2 [m]	Y1 [m]	Y2 [m]	Z1 [m]	Z2 [m]	[t]
Ship hull	0.0	36.1	-8.1	8.1	0.0	2.1	232.5
Work shop conttainer	3.0	5.5	-3.1	3.1	2.1	4.6	15.0
Power/control container	7.5	10.0	-3.1	3.1	2.1	4.6	15.0
Remainder	0.0	0.0	0.0	0.0	0.0	0.0	5.0
Excavator	29.1	35.1	-2.0	2.0	2.1	6.0	47.0
Ballast tank 1	0.0	4.5	-8.1	8.1	0.0	2.1	0.0
Ballast tank 2	4.5	12.0	-8.1	0.0	0.0	2.1	0.0
Ballast tank 3	4.5	12.0	0.0	8.1	0.0	2.1	0.0
Ballast tank 4	12.0	18.0	-8.1	0.0	0.0	2.1	96.4
Ballast tank 5	12.0	18.0	0.0	8.1	0.0	2.1	96.4
TOTAL							**527.3**

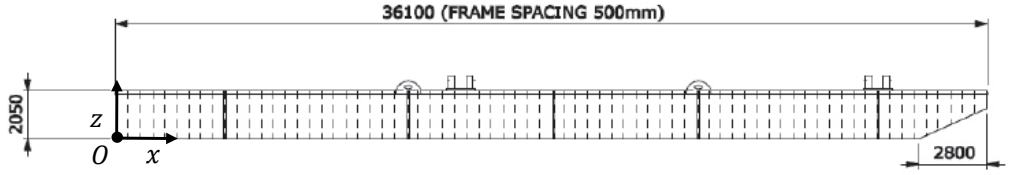

SIDE VIEW

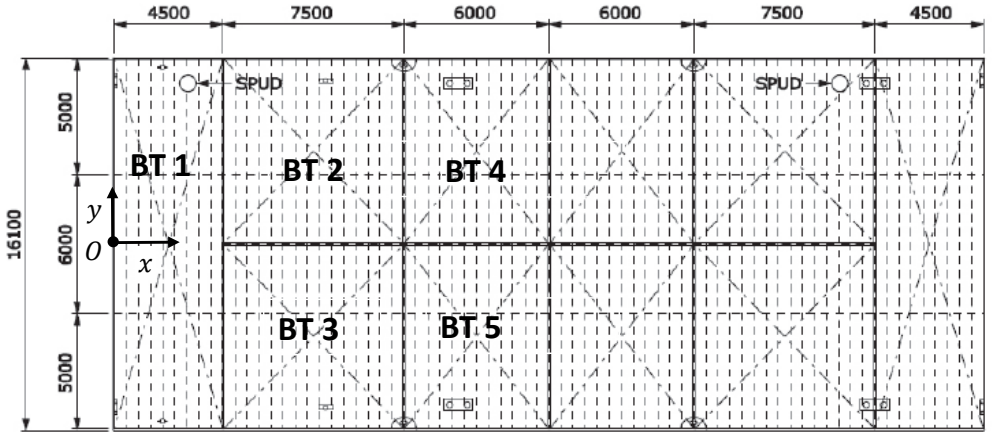

TOP VIEW DECK LEVEL

Appendix G

Tolerance calculation

In this appendix, the information used to calculate the tolerances is elaborated. As already discussed, the tolerances are determined from guidelines on excavators and standard pin-shaft connections. The tolerances are divided in two different components: pin-shaft joints and swing bearing.

G.1 Pin-shaft joints

G.1.1 Lateral

In case the excavator arm is laterally loaded by a small forces as depicted in the figure below, the pin in the shaft will allow certain angle on the stick relative to the boom, dependent on the clearance of the hole. This is schematically shown in the figure below.

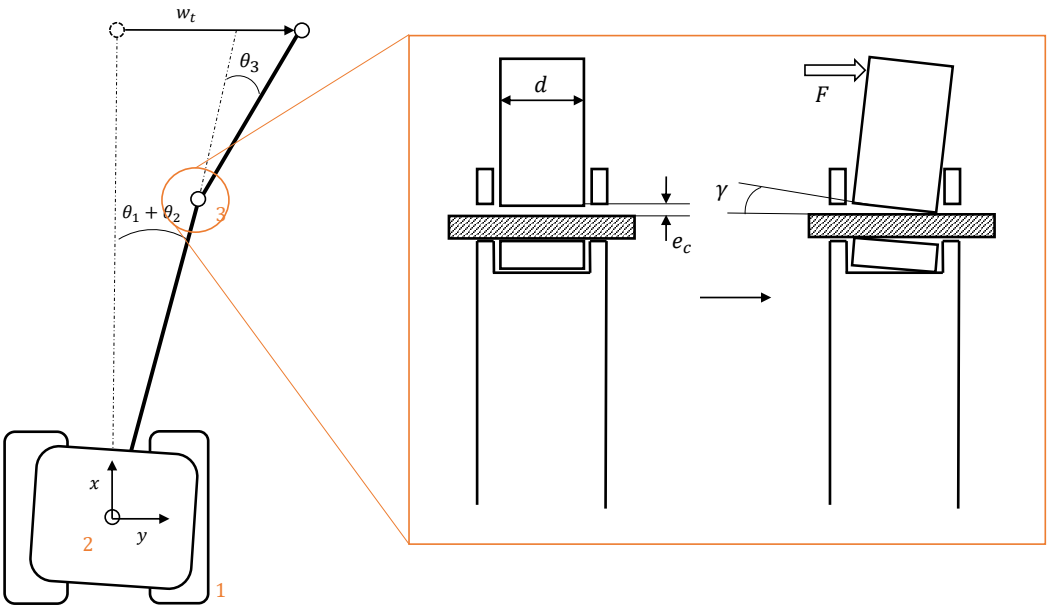

Figure G.1

The clearance e_c is determined by ISO guidelines. For this case, the preferred fit is ISO code H11/d11. This code is used for free running fits not for use where accuracy is essential, but good for large temperature variations, high running speeds, or heavy journal pressures. A table below shows the clearance for some typical hole and shaft size ranges used in current study.

TABLE G.1: ISO tolerances for holes and shaft

Nominal size hole/shaft [mm]	Tolerance [μm]			Max clearance [μm]
		Shaft (H11)	Hole (d11)	
30 - 40	Max	+160	-240	400
	Min	0	-80	
40 - 80	Max	+190	-290	480
	Min	0	-100	
80 - 120	Max	+220	-340	560
	Min	0	-120	

The worst case angle of rotation around the z-axis γ_z can now be calculated with the help of these clearances as:

$$\gamma_z = \frac{(FoS \cdot e_c \cdot 360)}{2\pi \cdot b} \tag{G.1}$$

where

FoS = Factor of safety for wear and temperature changes = 1.5
b = Width of the rotating components [mm]

In the figure above, the rotating component is the stick of which the dimension can be found in Appendix E.

G.1.2 Longitudinal

In case the excavator arm is longitudinal loaded by a small forces as depicted in the figure below, the pin in the shaft will allow certain angle on the stick relative to the boom, dependent on the clearance of the hole. This is schematically shown in the figure.

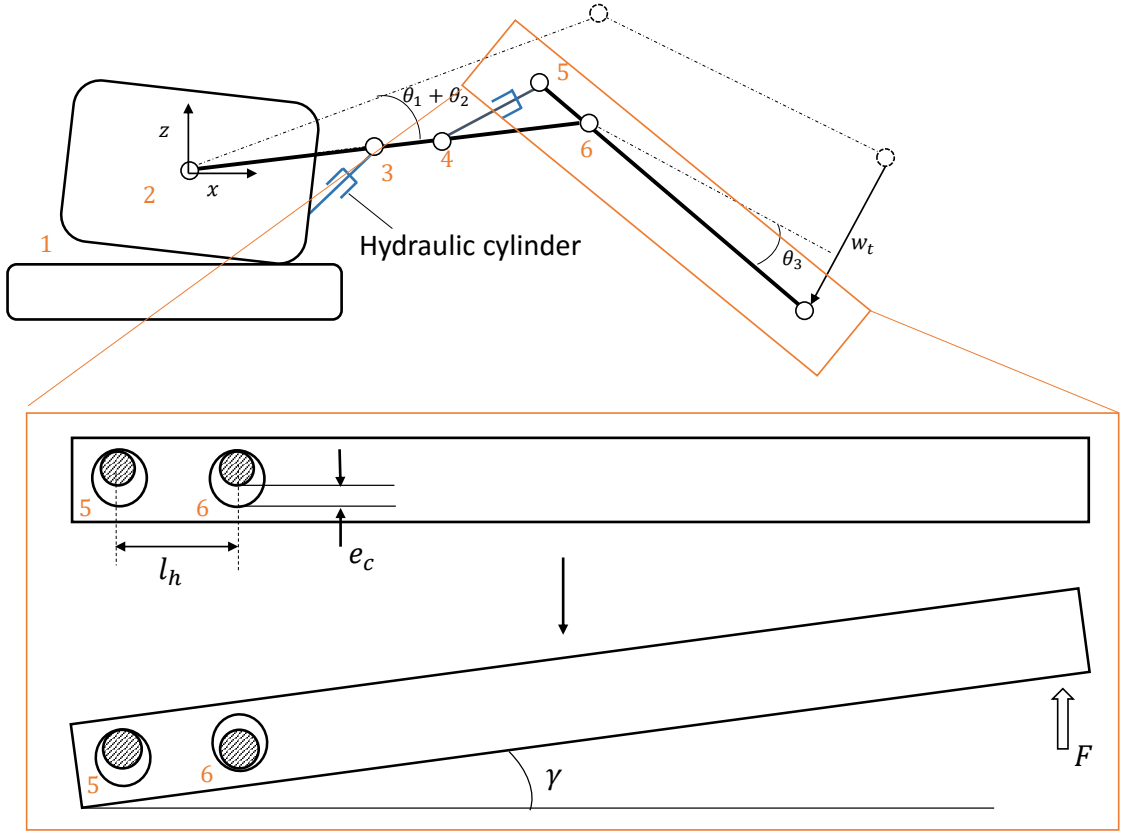

FIGURE G.2

Table G.1 is used to determine the clearance of the holes. If a small force is applied at the end of the stick, as depicted in the figure, the stick will rotate for example around joint 5. Hereby it will mobilize the clearance in joint six. The rotation over the y-axis which the stick will obtain in the worst case can be calculated with:

$$\gamma_y = \frac{(FoS \cdot e_c \cdot 360)}{2\pi \cdot l_h} \tag{G.2}$$

where

FoS = Factor of safety for wear and temperature changes = 1.5
l_h = Distance between the two joints [mm]

This can be done for each joint, since each clearance in the shaft and holes can result in a certain rotation of either the boom or stick.

G.2 Swing bearing

An excavator uses a swing bearing to rotate the base relative to the undercarriage. A sketch of a swing bearing is shown in figure G.3. The swing bearing comprises a couple of tolerances which can lead to an offset of the excavator tip:

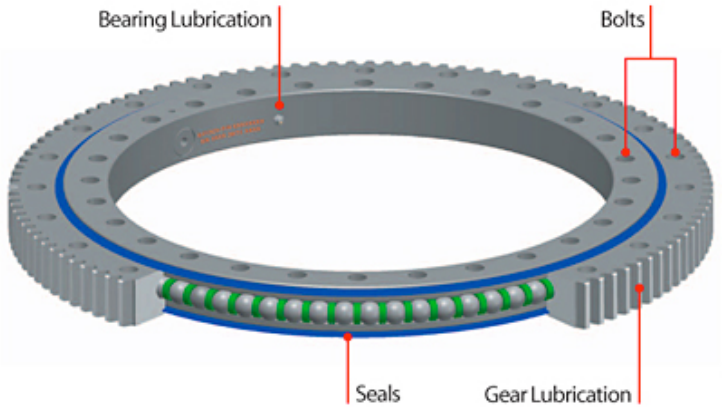

FIGURE G.3

G.2.1 Rotating clearance / Gear tolerance

The gear of the swing bearing have a certain backlash as depicted in the figure below. Following the specifications sheets of the swing bearing of the excavator, the maximum gear tolerance is defined as $J = 0.65$ mm.

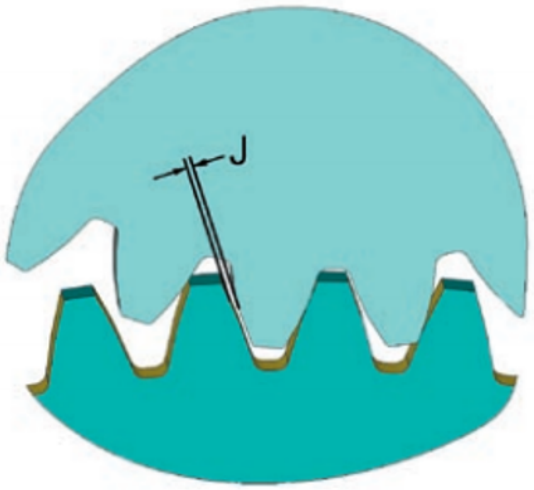

FIGURE G.4

The rotation of the excavator base relative to the undercarriage around the z-axis can be calculated with:

$$\gamma_z = \frac{(e_t \cdot 360)}{2\pi \cdot D_r} \tag{G.3}$$

where

FoS	=	Factor of safety for wear and temperature changes = 1.5
J	=	Maximum gear clearance as depicted in G.4 [mm]
D_r	=	Diameter of the raceway in the swing bearing [mm]

G.2.2 Tilting clearance

The roller balls in the raceway of the swing bearing have certain geometric tolerances. Furthermore raceway wear of the roller bearing leads to increased tilting clearance shown in the figure below. The limits for permissible increase in tilting clearance are given in the following table at which the bearing must always be exchanged.

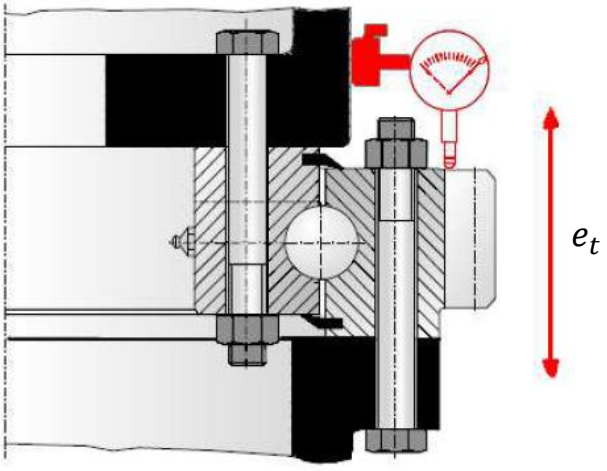

FIGURE G.5

Maximum allowed increase in tilting clearance						
Rolling element diameter (mm)	12	16	20	25	32	40
Ball supporting clearance (mm)	1.02	1.16	1.30	1.48	1.72	2.00
Roller supporting clearance (mm)	0.18	0.25	0.32	0.40	0.52	0.65
Rolling element diameter (mm)	45	50	60	70	80	100
Ball supporting clearance (mm)	2.18	2.35	2.70	3.05	3.40	4.10
Roller supporting clearance (mm)	0.74	0.82	0.99	1.16	1.33	1.67

FIGURE G.6

These values are used to calculate the maximum rotation of the excavator base, due to tilting as depicted in top sketch (marked with a 1) of figure G.2. The rotation is assumed to only result in a rotation in longitudinal direction. In lateral direction (figure G.1) the rotation due

to tilting only results in a rotation of the tip and no translations. The rotation of the excavator base around the y-axis can be calculated by:

$$\gamma_y = \frac{(e_t \cdot 360)}{2\pi \cdot D_r} \tag{G.4}$$

where

e_t = Maximum tilting clearance as given in table G.6 [mm]
D_r = Diameter of the raceway in the swing bearing [mm]

In this case no factor of safety is used, since the values table G.6 are limits of the clearance when the lifetime of the bearing is over, thus this value already incorporates wear. For current, a rolling element of 40 mm is used, thus $e_t = 2$ mm, and the diameter of the swing bearing is $D_r = 1500$ mm.

Appendix H

Additional motion graphs

(Confidential)

Appendix I

AQWA input values

(Confidential)